

ADAPTIVE STEREOGRAPHIC MCMC

BY CAMERON BELL¹, KRZYSZTOF ŁATUSZYŃSKI¹, AND GARETH O. ROBERTS¹

¹*Department of Statistics, University of Warwick, United Kingdom*

In order to tackle the problem of sampling from heavy-tailed, high-dimensional distributions via Markov Chain Monte Carlo (MCMC) methods, [37] introduces the stereographic projection as a tool to compactify \mathbb{R}^d and transform the problem into sampling from a density on the unit sphere \mathbb{S}^d . However, the improvement in algorithmic efficiency, as well as the computational cost of the implementation, is significantly impacted by the parameters used in this transformation.

To address this, we introduce adaptive versions three stereographic MCMC algorithms - the Stereographic Random Walk (SRW), the Stereographic Slice Sampler (SSS), and the Stereographic Bouncy Particle Sampler (SBPS) - which automatically update the parameters of the algorithms as the run progresses. The adaptive setup allows to better exploit the power of the stereographic projection, even when the target distribution is neither centered nor homogeneous. Unlike Hamiltonian Monte Carlo (HMC) and other off-the-shelf MCMC samplers, the resulting algorithms are robust to starting far from the mean in heavy-tailed, high-dimensional settings. To prove convergence properties, we develop a novel framework for the analysis of adaptive MCMC algorithms over collections of simultaneously uniformly ergodic Markov operators, which is applicable to continuous-time processes, such as SBPS. This framework allows us to obtain \mathcal{L}^2 and almost sure convergence results, and a CLT for our adaptive stereographic algorithms.

1. Introduction. Markov chain Monte Carlo (MCMC) algorithms are used to approximate a given target distribution π on \mathbb{R}^d , which usually arises in the context of Bayesian inference. For this purpose, a Markov process is simulated that admits π as its stationary distribution, and we can use its empirical distribution to approximate π . It is therefore crucial that our algorithms quickly converge to stationarity and efficiently explore the entire target distribution.

From the Random Walk Metropolis algorithm (RWM) [25, 21] to Hamiltonian Monte Carlo (HMC) [27], many MCMC algorithms rely on local moves to explore the space. Even more sophisticated algorithms such as the Zig-Zag algorithm [7] or the Bouncy Particle Sampler (BPS) [10] only move at a fixed speed, although versions of these algorithms exist with non-constant speeds [9, 36]. If π is heavy-tailed, a large amount of probability mass will be spread far from the mode of the target. All of the above algorithms will struggle to efficiently mix when targeting such distributions because they have a tendency to get lost in one corner of the tails, follow near-Brownian dynamics, and take an eternity to return to the mode. These problems are only made worse by the “curse of dimensionality”: as the dimension d increases, more and more of the volume in \mathbb{R}^d is away from the mode, so there is “more” tail that needs efficiently exploring, whilst still needing to return quickly to the center of the target. Hence, heavy-tailed densities are a major obstacle for efficient posterior sampling. Another is multimodality, however we will primarily discuss the case where π is unimodal and

MSC2020 subject classifications: Primary 60J05, 60J20, 60J25, 65C05.

Keywords and phrases: adaptive Markov chain Monte Carlo, stereographic projection, random walk Metropolis, slice sampler, piecewise deterministic Markov process, uniform ergodicity, heavy-tailed distributions, blessings of dimensionality.

refer to many other works attempting to address the challenges of sampling from multimodal targets (e.g. [35, 28, 34] and references therein).

With this motivation, one solution is to attempt to transform the sample space onto a compact set, effectively removing the possibility of getting lost in the tails, then sample from the transformed target distribution on the new support. [37] achieve this via the stereographic projection: this map transforms Euclidean space \mathbb{R}^d onto \mathbb{S}^d/N , the unit sphere with the North pole $N = (0, \dots, 0, 1)$ removed. In this setting, N can be seen as the “image of ∞ ” under the map. Although \mathbb{S}^d/N is not compact, it is relatively compact and can easily be extended to the compact set \mathbb{S}^d . This allows algorithms to reach anywhere in the state space in bounded time using only local moves. The algorithms introduced in their paper are shown to be uniformly ergodic for a wide range of target distributions, including heavy-tailed targets, and even exhibit a “blessing of dimensionality” in ideal settings, converging to stationarity faster as d increases. Other papers, such as [24, 14], also introduce transformations of the state space to improve sampling properties, but these transformations do not yield the same geometric benefits as the stereographic projection.

However, having a compact support does not immediately lead to incredible sampling properties. If the target distribution π is poorly preconditioned, the probability mass will be concentrated on a very small part of the sphere, which locally looks to our algorithms like a very small version of \mathbb{R}^d and the potential benefits of using the stereographic projection are lost. We therefore parametrise the stereographic projection in order to attempt to evenly distribute the probability mass around \mathbb{S}^d . This is equivalent to preconditioning π to be centered and appropriately scaled before we apply the transformation.

With optimally chosen parameters, the probability mass becomes concentrated and uniformly spread around the equator of the sphere, which in turn improves the convergence and mixing of the MCMC algorithms. In practice, however, we will not know the optimal values for these parameters before running the process. A natural way of addressing this challenge is therefore to automatically update the parameters based on the history of the chain, and use these new, hopefully improved parameters in future transitions. This framework is known as adaptive MCMC, and is a relatively well-studied area [18, 2, 31, 3, 32, 33, 17, 11].

To address the issues of potentially poorly specified parameters in the stereographic algorithms, in this paper we create adaptive frameworks to update the parameters as we run our processes:

- we present adaptive versions of the 3 stereographic MCMC algorithms we discuss;
- we provide a unifying theorem giving appropriate conditions for a Strong Laws of Large Numbers (SLLN), \mathcal{L}^2 convergence and a CLT in each case;
- we prove this by showing that such a theorem holds when creating an adaptive version of any uniformly ergodic Markov process, whether discrete or continuous-time;
- we demonstrate benefits and robustness of the adaptive scheme on two synthetic examples.

In Section 2, we formally introduce the stereographic projection, then the three algorithms: the Stereographic Random Walk (SRW), the Stereographic Slice Sampler (SSS) and the Stereographic Bouncy Particle Sampler (SBPS). The SRW and SBPS were first presented in [37], and the SSS in [20] under the name geodesic slice sampler.

In Section 3, we present our adaptive versions of each of the algorithms. Our algorithms are based on the Adapting Increasingly Rarely (AIR) MCMC setup from [12, 23]. We state the main convergence results in Theorem 3.5. To theoretically justify the application of the AIR MCMC framework to our setting, we create a novel auxiliary process in Section 4, which we dub the segment chain. We show a SLLN, \mathcal{L}^2 convergence and a CLT for the segment chain, and show that any uniformly ergodic Markov process, whether discrete or continuous-time, inherits these results.

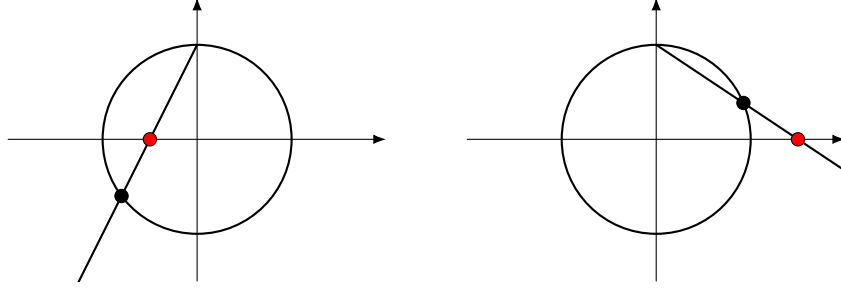


Fig 1: The stereographic projection between \mathbb{R} and \mathbb{S}^1 : given $x \in \mathbb{R}$, we draw a line between x (red) and the North pole $N = (0, 1)$, and define the projected point $z \in \mathbb{S}^1$ (black) to be point where the ray intersects the circle. We see that as $x \rightarrow \pm\infty$, $z \rightarrow N$.

Finally, in Section 5, we present two synthetic examples demonstrating the ability of our algorithms to adapt the parameters of the transformation and the improvement this yields in sampling properties. The second example in particular demonstrates the stereographic algorithms' ability to start deep in the tails of heavy-tailed, high-dimensional target distributions with poor initial parameter choices and still find the modal region. By comparison, HMC fails to make any progress in finding the mode.

2. Stereographic MCMC. We start by defining the stereographic projection, then the three algorithms: the Stereographic Random Walk (SRW), the Stereographic Slice Sampler (SSS), and the Stereographic Bouncy Particle Sampler (SBPS).

2.1. The Stereographic Projection. The stereographic projection is a diffeomorphism from the punctured unit sphere $\mathbb{S}^d / \{N\}$, where $N = (0, \dots, 0, 1)$ is the “North pole”, to \mathbb{R}^d . Figure 1 presents the geometric intuition of the stereographic projection in the case $d = 1$.

Generalising to higher dimensions, and given a vector $\mu \in \mathbb{R}^d$ and a positive definite matrix $\Sigma \in \mathbb{R}^{d \times d}$, the (preconditioned) stereographic projection of a point $z \in \mathbb{S}^d$ gives:

$$(2.1) \quad x = \Sigma^{1/2} \left(\frac{z_1}{1 - z_{d+1}}, \dots, \frac{z_d}{1 - z_{d+1}} \right) + \mu,$$

and:

$$(2.2) \quad \begin{aligned} z_{1:d} &= \frac{2\Sigma^{-1/2}(x - \mu)}{\|\Sigma^{-1/2}(x - \mu)\|^2 + 1}, \\ z_{d+1} &= \frac{\|\Sigma^{-1/2}(x - \mu)\|^2 - 1}{\|\Sigma^{-1/2}(x - \mu)\|^2 + 1}. \end{aligned}$$

This can be thought of as mapping from z to $\tilde{x} = \frac{z_{1:d}}{1 - z_{d+1}}$, then preconditioning to obtain $x = \Sigma^{1/2}\tilde{x} + \mu$. In other words, before we draw our ray from N to x , we perform an affine transformation by translating x by $-\mu$ and scaling via $\Sigma^{-1/2}$. Although mathematically equivalent, it is preferable to apply the transformations to \mathbb{R}^d rather than turn \mathbb{S}^d into an ellipsoid so that the symmetry and constant curvature of the unit sphere is retained for simplicity of the resulting MCMC implementations. However, when communicating geometric intuition, talking instead about the equivalent transformation of adjusting the shape and location of the sphere is often convenient.

Setting $\gamma = (\mu, \Sigma) \in \Gamma$ as the parameter of the transformation and Γ as full parameter space, we write

$$(2.3) \quad x = \text{SP}_\gamma(z) \quad \text{and} \quad z = \text{SP}_\gamma^{-1}(x)$$

for the stereographic projection map (2.1) and its inverse (2.2).

Under the stereographic projection, N can be thought of as the image of ∞ in \mathbb{S}^d , folded into a single point, because as $\|x\| \rightarrow \infty$ in any way, $z = \text{SP}_\gamma^{-1}(x) \rightarrow N$. Moreover, we can travel vast distances in \mathbb{R}^d by taking a very small step within the vicinity of the North Pole in \mathbb{S}^d . This will allow our MCMC algorithms to quickly explore the tails of the target distribution and then easily return to the high-probability region.

Using the Jacobian of the stereographic projection, $J_{\text{SP}_\gamma}(x) \propto (1 + \|\Sigma^{-1/2}(x - \mu)\|^2)^d$, we transform the target density $\pi(x)$ on \mathbb{R}^d to the following density on \mathbb{S}^d :

$$(2.4) \quad \begin{aligned} \pi_\gamma(z) &\propto \pi(x) (1 + \|\Sigma^{-1/2}(x - \mu)\|^2)^d \\ &\propto \pi(x) (1 - z_{d+1})^{-d}, \end{aligned}$$

where x and z are related by (2.3). For example, if $\pi(x) \propto (d + \|x\|^2)^d$ a multivariate t -distribution (MtD) with $\nu = d$ degrees of freedom (DoF), then π_γ is uniform on \mathbb{S}^d when $\mu = 0_d$ and $\Sigma = dI_d$.

2.2. Markov Processes on the Sphere. Given the transformed density π_γ on \mathbb{S}^d , we now discuss algorithms to efficiently sample from densities on the unit sphere. Since \mathbb{S}^d is compact, we will see in Section 4.2 that our stereographic MCMC algorithms can be uniformly ergodic, even in cases where π has polynomial tails in \mathbb{R}^d .

2.2.1. The Stereographic Random Walk. We start with the SRW, a RWM algorithm on the sphere. This algorithm was introduced in [37] under the name stereographic projection sampler. We rename it to SRW for more consistent terminology and easier differentiation of acronyms.

Given a position $z \in \mathbb{S}^d$, we propose the next point by taking a Gaussian step in the hyperplane tangent to \mathbb{S}^d at z , then normalising the vector to return to \mathbb{S}^d . This proposal scheme is shown in Figure 2.

To implement this, given $Z_n = z$, we sample $\tilde{dz} \sim \mathcal{N}(0_{d+1}, h^2 I_{d+1})$ and set $dz = \tilde{dz} - (z \cdot \tilde{dz})z$ to be the Gaussian step orthogonal to z . Here $(\cdot \cdot)$ denotes the standard inner product. We then let our proposal point be $z' = \frac{z + dz}{\|z + dz\|}$. The symmetrical nature of the Gaussian distribution ensures the proposal kernel $q(z, z')$ is reversible with respect to the uniform measure on \mathbb{S}^d :

$$(2.5) \quad q(z, z') = q(z', z).$$

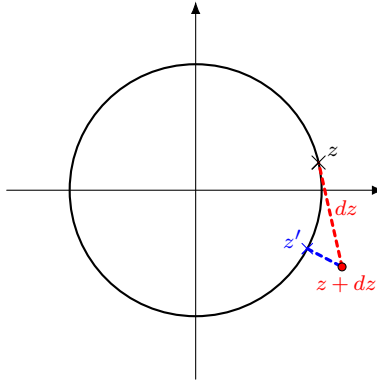


Fig 2: An SRW proposal

Algorithm 1 The Stereographic Random Walk

Input: Target density π on \mathbb{R}^d , $X_0 \in \mathbb{R}^d$, parameters $\gamma \in \Gamma$, $h > 0$, $Z_0 = \text{SP}_\gamma^{-1}(X_0)$

Output: $\{(X_n, Z_n)\}_{n \in \mathbb{N}}$ [2pt]

For: $n = 0, 1, \dots$:

- Sample $\tilde{dz} \sim \mathcal{N}(0_{d+1}, h^2 I_{d+1})$ in \mathbb{R}^{d+1} , and set $dz = \tilde{dz} - (\tilde{dz} \cdot Z_n) Z_n$
- Set $z' = \frac{Z_n + dz}{\|Z_n + dz\|}$, and set $Z_{n+1} = z'$ with probability:

$$\min\left(\frac{\pi_\gamma(z')}{\pi_\gamma(Z_n)}, 1\right) = \min\left(\frac{\pi(x')(1 - z'_{d+1})^{-d}}{\pi(X_n)(1 - Z_{n,d+1})^{-d}}, 1\right),$$

where $x' = \text{SP}_\gamma(z')$. Otherwise, set $Z_{n+1} = Z_n$

- Set $X_{n+1} = \text{SP}_\gamma(Z_{n+1})$
-

We then accept z' as the new position with probability $\min(\frac{\pi_\gamma(z')}{\pi_\gamma(Z_n)}, 1)$, since the proposal is reversible. The overall algorithm is given in Algorithm 1.

From Equation (2.5), we see that this is indeed a RWM algorithm, and therefore has invariant measure π_γ on \mathbb{S}^d . The projection of the sample path onto \mathbb{R}^d will therefore have stationary distribution π . Furthermore, the SRW is simultaneously uniformly ergodic, even when targeting densities as heavy-tailed as a MtD with at least d DoF (see Lemma 4.1).

2.2.2. The Stereographic Slice Sampler. [20] present the geodesic slice sampler as a method for sampling from distributions on \mathbb{S}^d . We repurpose it as the SSS and apply it to π_γ .

From a position $z \in \mathbb{S}^d$, we start by sampling v uniformly from the set $\{z\}^\perp = \{v \in \mathbb{S}^d : v \cdot z = 0\}$, i.e. $v \sim p(\cdot|z)$ where:

$$(2.6) \quad p(dv|z) = \frac{dv}{|\mathbb{S}^{d-1}|} \mathbb{1}(v \cdot z = 0),$$

to define a geodesic of the form $\{z \cos(\theta) + v \sin(\theta) : \theta \in [0; 2\pi)\}$. We also define the space of orthonormal pairs (z, v) as:

$$(2.7) \quad \mathbb{S}^d \perp \mathbb{S}^d = \{(z, v) \in \mathbb{S}^d \times \mathbb{S}^d : z \cdot v = 0\}.$$

We then aim to perform a slice sampling step targeting the measure on the one dimensional geodesic with density proportional to π_γ . We start by sampling $t \sim U(0, \pi_\gamma(z))$, then wish to sample a new position z' uniformly from the superlevel set:

$$(2.8) \quad L_{z,v}(t) = \{z' = z \cos(\theta) + v \sin(\theta) : \theta \in [0, 2\pi), \pi_\gamma(z') > t\}.$$

In practice, exact sampling from the uniform distribution on $L_{z,v}(t)$ requires rejection sampling and can be very inefficient. To improve efficiency, at each step [20] instead uses an adaptive rejection sampling algorithm, referred to as the shrinkage procedure. This process is explicitly stated in Algorithm 2, and depicted geometrically in Figure 3.

The shrinkage procedure, which we denote $\text{Shrink}(z, v, t)$, is then incorporated into a full Markov kernel: given a current position $Z_n = z \in \mathbb{S}^d$, we sample $t \sim U(0, \pi_\gamma(z))$, $v \sim p(\cdot|z)$, then sample $Z_{n+1} \sim \text{Shrink}(z, v, t)$. We summarise this in Algorithm 3. [20] prove in Proposition 15 that the shrinkage procedure is reversible with respect to the uniform distribution on $L_{z,v}(t)$, and therefore that the SSS kernel is π_γ reversible, and so has the correct stationary distribution. Furthermore, the SSS is simultaneously uniformly ergodic, even when targeting densities as heavy-tailed as a MtD with at least d DoF (see Lemma 4.2).

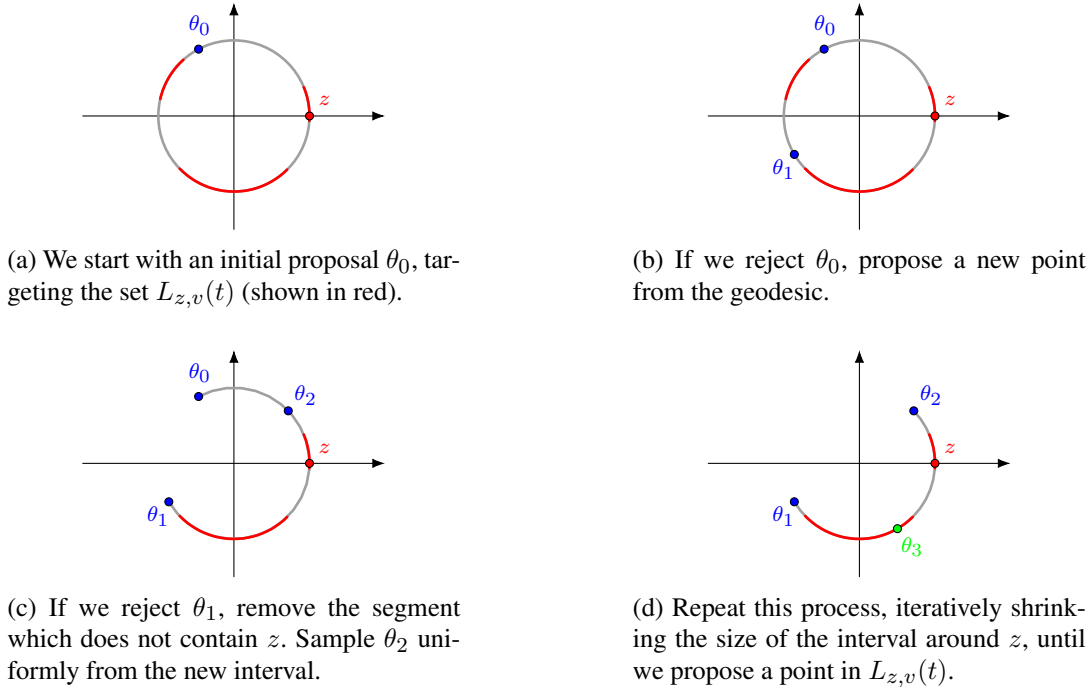


Fig 3: The Shrinkage Procedure for the Stereographic Slice Sampler: consider an initial position z and a geodesic defined by some v . The set $L_{z,v}(t)$ is shown in red, and the search interval by using sequentially shrinks based on the rejected points.

2.2.3. The Stereographic Bouncy Particle Sampler. Our last algorithm, the SBPS, was introduced in [37], and is a Piecewise Deterministic Markov Process (PDMP) targeting π_γ . Unlike the previous two algorithms, it is defined as a continuous-time process over $\mathbb{S}^d \perp \mathbb{S}^d$, as defined in equation (2.7), where the position z is considered to be our sample point, and the velocity v is a latent variable used to explore the space. Given an initial pair $(z_0, v_0) \in \mathbb{S}^d \perp \mathbb{S}^d$, the process evolves deterministically along a geodesic, according to the dynamics:

$$(2.9) \quad \begin{aligned} z(t) &= z_0 \cos(t) + v_0 \sin(t), \\ v(t) &= v_0 \cos(t) - z_0 \sin(t). \end{aligned}$$

We then introduce two types of random events at which we change the velocity v . Once an event occurs, we resume our deterministic dynamics according to Equation (2.9), but with the new velocity.

Algorithm 2 The Shrinkage Procedure for the Stereographic Slice Sampler

Input: Target density p on \mathbb{S}^d , orthonormal pair $(z, v) \in \mathbb{S}^d \perp \mathbb{S}^d$, level $t \in (0, p(z))$

Output: $z' \in L_{z,v}(t)$

Initialisation: Sample $\theta \sim U(0, 2\pi)$, and set $\theta_{\max} = \theta$, $\theta_{\min} = \theta - 2\pi$

While $p(z \cos(\theta) + v \sin(\theta)) \leq t$:

- **If** $\theta < 0$: Set $\theta_{\min} = \theta$
- **Else:** Set $\theta_{\max} = \theta$
- Resample $\theta \sim U(\theta_{\min}, \theta_{\max})$

Return: $z' = z \cos(\theta) + v \sin(\theta)$.

Algorithm 3 The Stereographic Slice Sampler

Input: Target density π on \mathbb{R}^d , $X_0 \in \mathbb{R}^d$, parameter $\gamma \in \Gamma$, $Z_0 = \text{SP}_\gamma^{-1}(X_0)$

Output: $\{(X_n, Z_n)\}_{n \in \mathbb{N}}$

For $n = 0, 1, \dots$:

- Sample $T_n \sim U(0, \pi_\gamma(Z_n))$, and $V_n \sim p(\cdot | Z_n)$
 - Sample $Z_{n+1} \sim \text{Shrink}(Z_n, V_n, T_n)$ according to the shrinkage procedure in Algorithm 2
 - Set $X_{n+1} = \text{SP}_\gamma(Z_{n+1})$
-

Bounce events occur according to an inhomogeneous Poisson process with rate $\chi(t) = \lambda(z(t), v(t))$, where:

$$(2.10) \quad \lambda(z, v) = \max \left[0, -v \cdot \nabla_z \log \pi_\gamma(z) \right],$$

which is equal to $\left(-\frac{d \log \pi_\gamma(z(t))}{dt} \right)^+$ at $(z(t), v(t))$. Bounce events therefore cannot occur if $\log \pi_\gamma(z(t))$ is increasing and are expected to occur sooner the faster $\log \pi_\gamma(z(t))$ is decreasing.

For a bounce event at (z, v) , we update the velocity v by reflecting its component in the direction of the gradient of $\log \pi_\gamma$ to:

$$(2.11) \quad v' = v - 2 \frac{v \cdot \tilde{\nabla}_z \log \pi_\gamma(z)}{\|\tilde{\nabla}_z \log \pi_\gamma(z)\|^2} \tilde{\nabla}_z \log \pi_\gamma(z),$$

where the $\tilde{\nabla}_z$ operator refers to the portion of the gradient which is tangent to the sphere at z , and is expressed by:

$$(2.12) \quad \tilde{\nabla}_z U(z) = \nabla_z U(z) - (z \cdot \nabla_z U(z))z,$$

for an arbitrary function U . Geometrically, the path of the particle around bounce events is described in Figure 4.

We let $R(z)$ be the matrix:

$$(2.13) \quad R(z) = I_{d+1} - 2 \frac{\tilde{\nabla}_z \log \pi_\gamma(z) \tilde{\nabla}_z \log \pi_\gamma(z)^T}{\|\tilde{\nabla}_z \log \pi_\gamma(z)\|^2},$$

so that $v' = R(z)v$ for a bounce event at (z, v) .

Our second type of event, refreshment events, occurs according to a homogeneous Poisson process with constant rate $\lambda_{\text{ref}} > 0$ independently of the current state of the process. For a

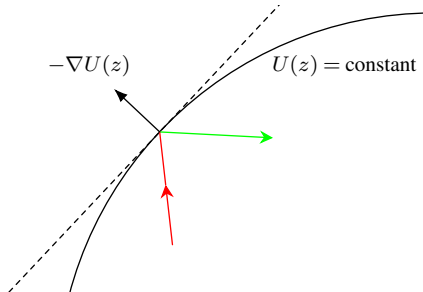
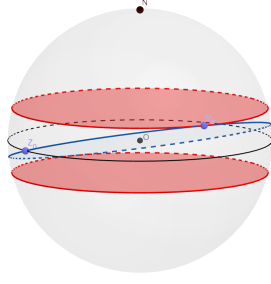
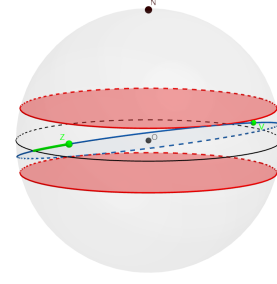


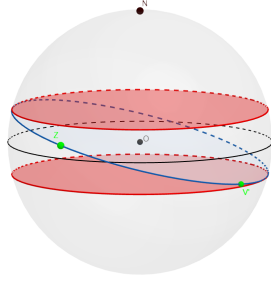
Fig 4: Illustration of a Bounce Event. Here, the target density is taken to be of the form $\pi_\gamma(z) \propto \exp(U(z))$ for some function $U(z)$. The particle initially travels “downhill” along the red path before bouncing at a specific time. At the event time, the particle lies on the black contour of $U(z)$ and “bounces” away from it.



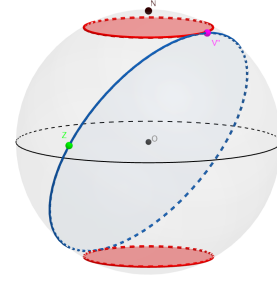
(a) Any geodesic is constrained to a certain region around the equator.



(b) Running the dynamics SBPS keeps us there.



(c) Bounce events cannot change these bounds on the latitude.



(d) Refreshment events allow the process to access the entire sample space.

Fig 5: SBPS Bounce Events do not allow the path to leave the vicinity of the equator when targeting a spherically symmetrical distribution, such as a $\mathcal{N}(0_d, I_d)$. Refreshment events are then required to ensure irreducibility.

refreshment event at (z, v) , we sample $v' \sim p(\cdot|z)$ uniformly from $\{z\}^\perp$, as in Equation (2.6), therefore choosing a new geodesic to follow uniformly at random. As with the Euclidean BPS, including independent refreshments is necessary for irreducibility of the algorithm, as shown in Figure 5.

We denote (Z_t, V_t) the random position and velocity of the SBPS at time $t > 0$, and present the algorithm as a whole in Algorithm 4. Note that, computationally speaking, one will not be able to store or work with a continuous sample path. One can choose to either output a skeleton of the chain, sampled at regular time intervals of short length δ , or output the points at event times $\{(z^{(i)}, v^{(i)})\}_{i \in \mathbb{N}}$, although it is vital to note that the positions $z^{(i)}$ at event times are not distributed according to π_γ .

It is shown in [37] that the SBPS is ergodic, and its stationary distribution has density $\pi_\gamma(z) \times p(v|z)$ on $\mathbb{S}^d \perp \mathbb{S}^d$. Furthermore, the SRW is simultaneously uniformly ergodic, even when targeting densities as heavy-tailed as a MtD with at least $d - 1/2$ DoF (see Lemma 4.1).

3. Adaptive Stereographic Algorithms. Each of the above algorithms is parametrised by γ , the parameters of the stereographic projection, and potentially additional parameters determining the dynamics of the Markov kernel on \mathbb{S}^d (h for the SRW and λ_{ref} for the SBPS). The choices of these parameters can heavily impact algorithmic performance. In this section, we establish motivation for optimal choices of γ and introduce our adaptive versions of each of the 3 algorithms. We then find sufficient conditions for prove estimators produced by the adaptive algorithms to satisfy a SLLN, \mathcal{L}_2 convergence, and a CLT.

Algorithm 4 The Stereographic Bouncy Particle Sampler

Input: Target density π_γ on \mathbb{S}^d , $(Z_0, V_0) \in \mathbb{S}^d \perp \mathbb{S}^d$, refreshment rate λ_{ref} .

Output: $\{(Z_t, V_t)\}_{t \in [0, \infty)}$.

Initialisation: Set $(z^{(0)}, v^{(0)}) = (Z_0, V_0)$ and $s = 0$.

For $i = 0, 1, \dots$:

- Sample $\tau_{\text{ref}} \sim \text{Exp}(\lambda_{\text{ref}})$
 - Sample τ_{bounce} according to the first event of a Poisson process with rate function $t \mapsto \lambda(z(t), v(t))$, with $(z(t), v(t))$ given by Equation (2.9) initialised at $(z^{(i)}, v^{(i)})$, and $\lambda(z, v)$ as in Equation (2.10)
 - Set $\tau = \min(\tau_{\text{ref}}, \tau_{\text{bounce}})$, and $Z(t+s) = z^{(i)} \cos(t) + v^{(i)} \sin(t)$, $V(t+s) = v^{(i)} \cos(t) - z^{(i)} \sin(t)$ for all $t \in [0, \tau)$
 - Set $s = s + \tau$, $z^{(i+1)} = z^{(i)} \cos(\tau) + v^{(i)} \sin(\tau)$ and $\hat{v} = v^{(i)} \cos(\tau) - z^{(i)} \sin(\tau)$
 - **If** $\tau_{\text{ref}} < \tau_{\text{bounce}}$: sample $v^{(i+1)} \sim p(\cdot | z^{(i+1)})$
 - **Else:** set $v^{(i+1)} = R(z^{(i+1)})\hat{v}$ as per Equation (2.13)
-

3.1. The Equator as a High Probability Region. We will be interested in varying γ in order to optimally position and scale the sphere to match properties of the target distribution π . As discussed at the start of Section 2, this is equivalent to tuning the parameters of the affine preconditioning which we perform on \mathbb{R}^d before projecting onto \mathbb{S}^d .

To motivate the optimal choice of parameters, consider $X \sim \prod_{i=1}^d f(x_i)$ an iid product with $\mathbb{E}_f(X) = 0$ and $\mathbb{E}_f(X^2) = 1$. Then:

$$(3.1) \quad \frac{1}{d} \sum_{i=1}^d X_i^2 = 1 + \mathcal{O}_{\mathbb{P}}(d^{-\frac{1}{2}}).$$

Geometrically, as d increases, we see that the distribution of X will become more and more concentrated around a spherical shell of radius \sqrt{d} , as depicted in Figure 6.

As a consequence, taking $\mu = 0_d$ and $\Sigma = dI_d$:

$$(3.2) \quad Z_{d+1} = \frac{\frac{1}{d} \|X\|^2 - 1}{\frac{1}{d} \|X\|^2 + 1} = \mathcal{O}_{\mathbb{P}}(d^{-\frac{1}{2}}),$$

so that our sample points under π_γ will become concentrated around the equator. However, if γ is chosen poorly, the density is likely to become concentrated around one of the poles, as shown in Figure 7.

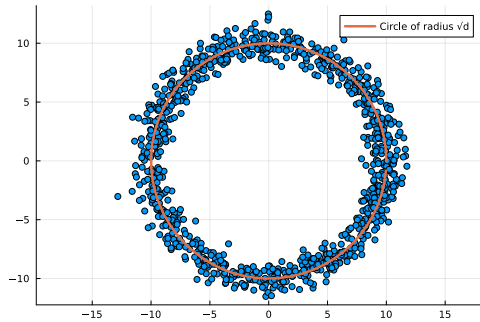
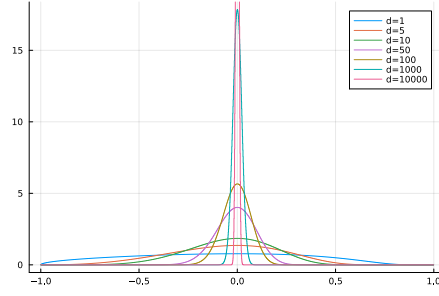
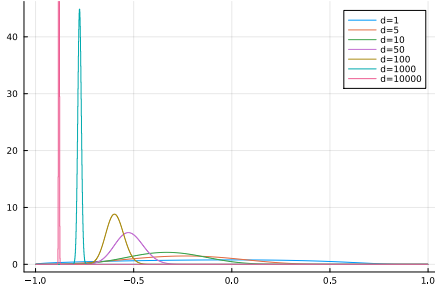


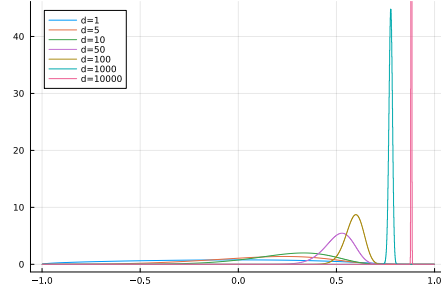
Fig 6: Visualisation of the norm of a $\mathcal{N}(0_d, I_d)$ distribution for $d = 100$. We project the points onto a 2 dimensional subspace to clearly show that points are likely to be at distance \sqrt{d} from the origin. In high dimensions, the circle is in reality a hyperspherical shell of radius \sqrt{d} .



(a) Taking $\Sigma = dI_d$, we see that π_γ becomes concentrated around the equator $z_{d+1} = 0$.



(b) Taking $\Sigma = d^{1.3}I_d$, we see that the mass moves towards the South pole. This is because the radius of the sphere we are using in the projection is too large.



(c) Taking $\Sigma = d^{0.7}I_d$, we see that the mass moves towards the North pole. This is because the radius of the sphere we are using in the projection is too small.

Fig 7: Plots of the marginal density of Z_{d+1} under π_γ , when $X \sim \mathcal{N}(0_d, I_d)$. We fix $\mu = 0$ and vary Σ .

We can therefore construct our algorithms to efficiently explore the equator, and tune our parameters to precondition the target by taking:

$$(3.3) \quad \mu = \mathbb{E}_\pi(X), \quad \Sigma = d \times \mathbb{E}_\pi((X - \mu)(X - \mu)^T).$$

Geometrically, if we consider μ and Σ as the center and shape of the sphere used in the stereographic projection, we are choosing our parameters so that the equator of the sphere intersects with \mathbb{R}^d along the spherical shell of high probability depicted in Figure 6.

These parameters are optimal as $d \rightarrow \infty$, as shown in Section 5.3 of [37], but it may not be the case for finite d that $\mathbb{E}_{\pi_\gamma}(Z_{d+1}) = 0$ when taking γ as in Equation (3.3). For example, for a MtD with d DoF, we want $\Sigma = dI_d = (d - 2)\text{Var}_\pi(X)$ to get a uniform distribution on the sphere and a target which is spread evenly around the equator. We therefore take:

$$(3.4) \quad \Sigma = c \times \mathbb{E}_\pi((X - \mu)(X - \mu)^T)$$

for $c > 0$ such that $\mathbb{E}_{\pi_\gamma}(Z_{d+1}) \approx 0$.

Each of our algorithms can be seen to have better mixing properties when γ is optimally chosen. For the SRW, the geometry of \mathbb{S}^d causes the proposed moves to naturally stay on the equator if that is where the chain lies and to drift back towards the equator if the chain is currently near either pole. Section 5 of [37] presents several results showing that if π is spherically symmetric then the SRW can be superefficient, when compared to the Euclidan RWM. It is shown that the acceptance probability goes to 1 as $d \rightarrow \infty$, even for a constant step size h . Since moves around the equator are then projected back onto \mathbb{R}^d by a factor

of roughly \sqrt{d} via Σ , we obtain a “blessing of dimensionality” where the expected jump distance of the SRW in Euclidean space will be $\mathcal{O}(d^{1/2})$ (i.e. mixing improves as d increases). By comparison, optimal Euclidean RWM steps will typically be $\mathcal{O}(d^{-1/2})$ as $d \rightarrow \infty$.

We give sketch arguments for the blessing of dimensionality in the case of the SSS or the SBPS. Both work from proposing moves along geodesics, which are more and more likely to remain in close proximity of the equator as d increases, and will always intersect the equator regardless of the current position. Thus, the algorithms will naturally stay within the vicinity of the equator if that is where they are, and will attempt to return to the equator in $\mathcal{O}(1)$ time even if the process is currently at one of the poles. If π is spherically symmetric and γ is appropriately chosen, we will therefore observe the same blessing of dimensionality as we get for the SRW where the expected distance traveled per step/unit time will also be $\mathcal{O}(d^{1/2})$.

Unlike the SRW, the SBPS and SSS also suffer computationally if π_γ is focused on a small subset of \mathbb{S}^d : the SBPS will require many bounce events to fight the drift back towards the equator, and the rejection sampling step in the SSS will reject many moves at every step before narrowing down the search interval. It is therefore all the more important for the parameter γ to be chosen appropriately when using these algorithms.

Since we do not know the expectations in Equation (3.3) in advance, it is of interest to create adaptive versions of any algorithm using the stereographic projection in order to automatically tune γ . It is worth mentioning that adaptations can also be performed for the other parameters, h and λ_{ref} . In the case of the SRW, we have already discussed that if π is spherically symmetric and γ is chosen correctly, then for any step size h the acceptance probability goes to 1. We therefore want to take h as large as possible. [37] also prove that if π is a non-Gaussian iid distribution, and γ is chosen according to Equation (3.3), then it is optimal to tune h to be $\mathcal{O}(d^{-1})$ such that we have an average acceptance rate of 0.234, as is the case for the Euclidean RWM algorithm [30]. It is therefore always appropriate to tune h to achieve an average acceptance rate of 0.234. Even if γ is poorly chosen, this will lead to a target distribution focused on a small corner of \mathbb{S}^d , which locally behaves like \mathbb{R}^d , so we still want to aim for the same acceptance rate.

The optimal refreshment rate for the SBPS is an open problem, but it is noteworthy that [8] shows that, for the Euclidean BPS, it is optimal in certain settings to have 78.1% of events be refreshment events. However, in a spherically symmetrical setting where we have very few bounces, this may lead to very small refreshment rates which could hurt the irreducibility of the process. We therefore recommend never taking a refreshment rate smaller than $\frac{1}{\pi}$, mimicking the No-U-Turn sampler’s intuition [22] of following the dynamics until we “turn around” at the other end of the geodesic.

3.2. The Algorithms. We now construct adaptive versions of the stereographic algorithms which automatically tune the parameters as they run, in order to improve performance. We established in Equation (3.3) what values we will be targeting with our estimators. However, as is the case for all adaptive MCMC algorithms, changing the transition scheme based on the full history of the sample path causes the Markov property to fail.

There is a vast literature for the construction and analysis of discrete-time adaptive MCMC algorithms with desirable asymptotic properties [2, 31, 3, 32, 33, 17, 11]. However, the literature on designing and studying continuous-time adaptive MCMC algorithms is lacking and the only such approach, [5], discretises the sample path to establish ergodicity. In this paper, we use the Adapting Increasingly Rarely (AIR) MCMC framework originally proposed in [12], and show how it can be applied to continuous-time adaptive processes. Crucially, this makes the setup identical for each of our algorithms.

We assume the lags t_k between adaptations are polynomially increasing, i.e. $\exists \beta > 0$ and $c \geq 1$ such that:

$$(3.5) \quad \frac{1}{c} k^\beta \leq t_k \leq c k^\beta,$$

Algorithm 5 AIR SRW

Input: Target density π on \mathbb{R}^d , $X_0^{(0)} \in \mathbb{R}^d$, initial parameters $\gamma_0 \in \Gamma$, $h_0 > 0$, sequence of adaptation lags $\{t_k\}_{k \in \mathbb{N}}$.

Output: $\{(Z_n^{(k)}, X_n^{(k)})\}_{0 \leq n \leq t_k}$, γ_k and h_k , for $k \in \mathbb{N}$.

For $k = 0, 1, \dots$:

- Run the SRW (Algorithm 1) for t_{k+1} time units to get

$$\{(Z_n^{(k+1)}, X_n^{(k+1)})\}_{0 \leq n \leq t_{k+1}} \sim \text{SRW}(\pi, X_{t_k}^{(k)}, \gamma_k, h_k)$$

- Update parameters to γ_{k+1}, h_{k+1} using $\{(Z_n^{(k+1)}, X_n^{(k+1)})\}_{0 \leq n \leq t_{k+1}}$

and define the adaptation times $T_k = \sum_{i=1}^k t_i$ with $T_0 = t_0 = 0$.

We proceed by running the process with the parameter γ_k fixed for $t \in [T_k, T_{k+1})$. At each time T_{k+1} , we update the parameter to γ_{k+1} based on the sample path so far and the previous parameter values. Algorithm 5 outlines the framework in the case of the SRW, with the corresponding algorithms for the SSS and SBPS being essentially identical, but replacing the SRW with their respective algorithms.

These AIR schemes have multiple benefits over the more commonly used adaptation schemes of adapting every step, or every k steps:

- Practically speaking, calculating the new adaptive parameters can be expensive, and reducing the frequency of the updates can have little impact on the mixing of the chain. For the stereographic MCMC algorithms, we will be trying to obtain an estimator for the square root of the covariance matrix to feed into our algorithms. Since there are no convenient iterative update schemes for this, we will need to recalculate a $d \times d$ covariance estimator and take its square root every time we adapt. In high dimensions, this can become very costly, so it is sensible to adapt more rarely as the process goes on, and we expect the estimators to converge.
- Theoretically speaking, adaptive MCMC algorithms can be tricky to analyse because using the history of the chain to inform future transitions causes the Markov property to break down. By keeping the parameters fixed for increasing lengths of time, we obtain a sequence of epochs that conditionally behave like standard Markov chains, and these sample paths become easier to control the longer they run for.

3.3. Asymptotic Results. We now present our main results for the convergence of estimators using the adaptive stereographic algorithms. Given any bounded function $f : \mathbb{R}^d \rightarrow \mathbb{R}$, we want to estimate $\pi(f) = \mathbb{E}_\pi(f(X))$. We are interested in the behaviour of the estimators:

$$(3.6) \quad \hat{f}_t^{\text{disc}} = \frac{1}{t} \sum_{s=0}^{t-1} f(X_s), \quad \hat{f}_t^{\text{cont}} = \frac{1}{t} \int_{s=0}^t f(X_s) ds$$

depending on whether we are considering a discrete or continuous-time algorithm. Note also that for the sake of computation, we will generally evaluate estimators from SBPS sample paths by taking a discrete skeleton with small mesh size.

With this definition, it is clear why we need to move the path off of \mathbb{S}^d : since f is fixed on \mathbb{R}^d , the target function on \mathbb{S}^d would be:

$$(3.7) \quad f_\gamma(z) = f(\text{SP}_\gamma^{-1}(x)),$$

which changes as we update γ .

To obtain convergence results for the AIR stereographic algorithms, we make several assumptions.

ASSUMPTION 3.1. *The adaptation scheme for the parameter updates keeps $\gamma_i = (\mu_i, \Sigma_i)$ in the compact set $\Gamma_{r,R}$ for all i , where:*

$$\Gamma_{r,R} = \{\gamma \in \Gamma : \|\mu\| \leq R, r^2 \leq \rho_i \leq R^2, \forall i\},$$

for $0 < r < R$, and ρ_i are the eigenvalues of Σ .

For the AIR SRW, also assume $r \leq h_i \leq R$ for each h_i . For the AIR SBPS, also assume $r \leq \lambda_i \leq R$ for each λ_i .

This assumption restricts the parameters to a compact set, so that even if the adaptation scheme “goes wrong”, the parameters cannot cause arbitrarily poor mixing. As a benefit of the AIR framework, we can use any estimator for our parameters that respects Assumption 3.1, and will not require trickier conditions such as diminishing adaptations for our \mathcal{L}^2 or almost sure convergence.

ASSUMPTION 3.2. *The adaptation lags $t_k = \Theta(k^\beta)$ are chosen under mild conditions.*

This assumption allows the AIR setup to be used. The mild additional conditions arise through our method of proving the results and are simply a condition on the expression for the times t_k . These are of very little practical relevance, and we conjecture that simply assuming $t_k = \Theta(k^\beta)$ is sufficient. See Appendix A.2 for more details.

For our assumptions on the target distribution, we will need a slightly different assumption for the SRW and SSS to the assumption for the SBPS. For the SRW and SSS, we need:

ASSUMPTION 3.3. *The target density π is positive, continuous, and satisfies:*

$$\limsup_{\|x\| \rightarrow \infty} \left(\pi(x)(\|x\|^2 + 1)^d \right) < \infty.$$

This assumption ensures that π_γ is bounded over \mathbb{S}^d . Our Markov chains are then targeting a distribution with a bounded density and a compact support, leading to uniform ergodicity (see Lemmas 4.1 and 4.2). If this condition fails, the chains could get stuck in the vicinity of the North pole for arbitrarily long times.

Note that this condition is satisfied for distributions with relatively heavy tails, such as MtD with at least d DoF.

Since the SBPS works off of $\nabla_z \log \pi_\gamma$, we need a different condition:

ASSUMPTION 3.4. *The target density π is positive, continuously differentiable and satisfies:*

$$\limsup_{\|x\| \rightarrow \infty} \left(x \cdot \nabla_x \log \pi(x) + R \|\nabla_x \log \pi(x)\| \right) + 2d < \frac{1}{2},$$

for some $R > 0$.

This assumption also ensures that the North pole does not become an inescapable singularity, and is sufficient for uniform ergodicity of the SBPS (see Lemma 4.3). It is also satisfied for distributions with relatively heavy tails, such as MtD with more than $d - \frac{1}{2}$ DoF.

Although these are sufficient conditions to expect good convergence results, we do not require them for the algorithms to still perform well, and significantly outperform non-stereographic counterparts. Indeed, neither Assumption 3.3 nor Assumption 3.4 hold in the example discussed in Section 5.2, in which we see that the stereographic methods significantly outperform HMC.

With these assumptions, we can then obtain the following result on the behaviour of \hat{f}_t :

THEOREM 3.5 (Asymptotics of \hat{f}_t). *Consider either of the estimators \hat{f}_t as given in Equation (3.6) for a bounded function $f : \mathbb{R}^d \rightarrow \mathbb{R}$, applied to the AIR SRW, SSS, SBPS, or any discrete skeleton of the SBPS, targeting the distribution π on \mathbb{R}^d .*

Under Assumption 3.1 for any $r < R \in (0, \infty)$, Assumption 3.2 for $\beta > 0$, and either Assumption 3.3 if we are working with the SRW or SSS, or assumption 3.4 for the SBPS, then for any initial position or parameters:

- *For any $\beta > 0$, and $0 \leq \epsilon < \min(\frac{1}{2}, \frac{\beta}{1+\beta})$, then as $t \rightarrow \infty$:*

$$t^\epsilon (\hat{f}_t - \pi(f)) \rightarrow 0, \quad \text{a.s. and in } \mathcal{L}^2.$$

In particular, a SLLN holds (by taking $\epsilon = 0$).

- *For $\beta > 1$, if $\gamma_i \xrightarrow{P} \gamma_\infty$, for some constant γ_∞ , such that the asymptotic variance $\sigma^2(\gamma_\infty) > 0$, and that $\sigma^2(\gamma)$ is a continuous function of γ , a CLT holds, i.e. as $t \rightarrow \infty$:*

$$\sqrt{t}(\hat{f}_t - \pi(f)) \rightarrow \mathcal{N}\left(0, \sigma^2(\gamma_\infty)\right), \quad \text{in distribution.}$$

This theorem combines elements from [12] and [23] to obtain the best of both results.

Note that although we express this in a unified way, the asymptotic variance $\sigma^2(\gamma)$ will depend on the choice of algorithm. Additionally, convergence of γ_i to some constant γ_∞ is given by part (a) of the theorem if we are using bounded empirical estimates for the optimal values of μ and Σ , as guided by Equation (3.3). However, this will not necessarily hold for estimators adapting h or λ_{ref} .

Comparing this result to other similar results, such as those discussed in [31], we see that despite significantly weaker assumptions on the adaptation scheme, we obtain almost sure and \mathcal{L}^2 convergence. The additional requirement on the convergence of the parameter and continuity of the asymptotic variance in the CLT result are comparable to those found in any similar result. We do not present a result on the ergodicity of the algorithm, i.e. whether $X_t \xrightarrow{D} \pi$ as $t \rightarrow \infty$, as these would bring identical conditions to more general results already found in the literature [31].

Although the sampling mechanisms for our three algorithms are very different, we obtain essentially identical convergence results. This is an artifact of our proof, in which we use the simultaneous uniform ergodicity of the processes to create a unifying auxiliary Markov chain which is much easier to work with than any of our original processes.

4. The Segment Chain for Uniformly Ergodic Markov Processes. We have already discussed the AIR framework and its intuitive appeal. However, the theory presented in [12] assumes a discrete-time chain, with a 1-step small set condition and simultaneous geometric ergodicity. Instead, the stereographic algorithms are all simultaneously uniformly ergodic, and the SBPS lives in continuous-time. [23] does give results for the simultaneously uniformly ergodic case for discrete-time algorithms, but also does not discuss either \mathcal{L}^2 convergence or a CLT.

In this section, we present a novel auxiliary process, the segment chain, which gives a unified framework for analysing any uniformly ergodic Markov process. This framework is particularly useful for the study of continuous-time chains, where notions of splitting, excursions, and regenerations are not as well studied. We use it to prove the asymptotic results in Theorem 3.5.

4.1. A Markov chain in the space of paths. Consider a continuous-time Markov process $\{X_t\}_{t \geq 0}$ on a sample space χ and its parametrised associated transition semigroup $\{P_\gamma^t\}_{t \geq 0}$, where $\gamma \in \Gamma$ is a parameter. Let π_γ be the stationary measure of P_γ (these need not be equal). Unfortunately, this notation clashes with the π_γ from the stereographic projection, and these two do not necessarily equate in our setting. For example, for the SBPS, this stationary distribution would be the joint distribution of X in \mathbb{R}^d and some latent velocity component whose distribution depends on γ . More on this in Section 4.2.

Suppose the process satisfies a simultaneous minorisation condition of the form:

$$(4.1) \quad P_\gamma^T(x, \cdot) \geq \epsilon \nu(\cdot), \quad \forall x \in \chi, \gamma \in \Gamma,$$

with $T > 0$, $\epsilon > 0$, and ν a probability measure on χ , all independent of γ . This implies that regardless of the values of X_t or γ , we have probability ϵ to get $X_{t+T} \sim \nu$ independently of $\{X_s\}_{0 \leq s \leq t}$. Such a condition is equivalent to the following, more traditional expression for uniform ergodicity of the process:

$$(4.2) \quad \|P_\gamma^t(x, \cdot) - \pi\|_{\text{TV}} \leq C \rho^t, \quad \forall x \in \chi, \gamma \in \Gamma,$$

where $t > 0$, and $C > 0$, $\rho \in (0, 1)$ are constants independent of γ .

We then define the segment chain $\{\Phi_n\}_{n \in \mathbb{N}}$ to be a discrete-time Markov chain with $\Phi_n : [0, T] \rightarrow \chi$ such that:

$$(4.3) \quad \Phi_n(t) = X_{nT+t}.$$

The segment chain $\{\Phi_n\}_{n \in \mathbb{N}}$ is then a Markov chain in the space of functions from $[0, T]$ to χ , which we shall simply call Ω .

If we have a discrete-time Markov chain satisfying the minorisation condition (4.1), we can instead take:

$$(4.4) \quad \Phi_n(t) = X_{nT+\lfloor t \rfloor},$$

to obtain the segment chain.

The crucial observation is that, using the minorisation condition (4.1), we can “split” the chain $\{\Phi_n\}_{n \in \mathbb{N}}$ such that, in a way we shall make rigorous later, for each n , with probability ϵ we have $\Phi_{n+1}(0) \sim \nu$ independently of $\Phi_0, \dots, \Phi_{n-1}$. This will allow us to divide sample paths into weakly dependent, identically distributed blocks, to which we can then apply standard techniques to get our LLNs and CLT results.

4.2. Simultaneous Uniform Ergodicity of Stereographic Algorithms. Before going further, we must ensure that the stereographic MCMC algorithms each satisfy a minorisation condition as described in Equation (4.1).

Since these Markov processes live in \mathbb{S}^d , which is compact, it is natural for them to exhibit uniform ergodicity properties similar to those of other algorithms targeting bounded densities with compact supports. As discussed alongside assumptions 3.3 and 3.4, the situation becomes slightly more complicated at the North pole N , since $\pi_\gamma(z)$ or $v \cdot \nabla_z \log \pi_\gamma(z)$ may not remain bounded as $z_{d+1} \rightarrow 1$.

Indeed, we have the following results for the SRW and SSS:

LEMMA 4.1 (SRW Minorisation Condition). *Suppose that $\gamma \in \Gamma_{r,R}$ for $0 < r < R < +\infty$. For P the Markov transition kernel for the SRW targeting π , and assuming π satisfies assumption 3.3, then $\exists \epsilon > 0$ and a probability measure ν on \mathbb{R}^d such that $\forall x \in \mathbb{R}^d$:*

$$P^3(x, \cdot) \geq \epsilon \nu(\cdot).$$

Furthermore, ϵ and ν can be chosen to be independent of γ .

LEMMA 4.2 (SSS Minorisation Condition). *Suppose that $\gamma \in \Gamma_{r,R}$ for $0 < r < R < +\infty$. For P the Markov transition kernel for the SSS targeting π , and assuming π satisfies assumption 3.3, then $\exists \epsilon > 0$ and a probability measure ν on \mathbb{R}^d such that $\forall x \in \mathbb{R}^d$:*

$$P(x, \cdot) \geq \epsilon \nu(\cdot).$$

Furthermore, ϵ and ν can be chosen to be independent of γ .

Note that ϵ and ν are implicitly different for the SRW and SSS. The proofs of these results involve constructing suitable sequences of events which allow the process to hit any given open ball of arbitrarily small radius, then lower bounding the probability of this sequence of events. We can then extend this lower bound to a measure on $(\mathbb{R}^d, \mathcal{B}(\mathbb{R}^d))$ by writing any set $A \in \mathcal{B}(\mathbb{R}^d)$ as a union of open balls. Most of the details can be found in [37] for the SRW or [20] for the SSS.

For the equivalent result in the case of the SBPS, we project the sample path $\{Z_t, V_t\}_{t \geq 0}$ onto Euclidean space to obtain a Markov process $\{X_t, W_t\}_{t \geq 0}$ with invariant distribution $\pi(x) \times p_\gamma(w|x)$ over $\mathbb{R}^d \times \mathbb{S}^{d-1}$. W_t is a unit vector related to the direction of the particle in \mathbb{R}^d , and is only necessary because $\{X_t\}_{t \geq 0}$ alone is not a Markov process.

It is noteworthy that here we are indeed considering a stationary distribution which changes with the parameter.

LEMMA 4.3 (SBPS Minorisation Condition). *Suppose that $\gamma \in \Gamma_{r,R}$ for $0 < r < R < +\infty$. For P the Markov transition kernel for the projected SBPS process $\{(X_t, W_t)\}_{t \geq 0}$ targeting π , and assuming π satisfies assumption 3.4, then $\exists T^* > 0$, $\epsilon > 0$ and a probability measure ν on $\mathbb{R}^d \times \mathbb{S}^{d-1}$ such that, $\forall T \geq T^*$, $\forall (x, w) \in \mathbb{R}^d \times \mathbb{S}^{d-1}$:*

$$P^T((x, w), \cdot) \geq \epsilon \nu(\cdot).$$

Furthermore, T^* , ϵ and ν can be chosen to be independent of γ .

The proof of Lemma 4.3 follows a Lyapunov function and small set proof. Most of the details can be found in [37]. Note that Lemma 4.3 gives a minorisation condition for the continuous-time SBPS, as well as any discrete-time skeleton of the SBPS.

With these minorisation conditions, we can map any of our algorithms' sample paths onto a segment chain with similar properties. We therefore only need to prove results in the general setting to obtain results for each of our algorithms, under appropriate conditions on π .

4.3. *Splitting and Regenerations for the segment chain.* We now return to our segment chain $\{\Phi_n\}_{n \in \mathbb{N}}$, as described in either Equation (4.3) or (4.4) for a general (continuous or discrete-time) Markov process X on a state space χ .

We let $\mathbb{Q}_\mu(\cdot; \gamma)$ be the probability measure on $(\Omega, \mathcal{B}(\Omega))$, the space of paths of length T , induced by the dynamics of $\{X_s\}_{0 \leq s \leq T}$ under parameter γ , subject to $X_0 \sim \mu$ for some probability measure μ on χ . If $X_0 = x$ a.s., we write this measure as $\mathbb{Q}_x(\cdot; \gamma)$. With this setup, we have that $\forall A \in \mathcal{B}(\Omega)$, $n \in \mathbb{N}$:

$$(4.5) \quad \mathbb{P}(\Phi_n \in A | \Phi_{0:(n-1)}) = \mathbb{Q}_{\Phi_{n-1}(T)}(A; \gamma).$$

We write:

$$(4.6) \quad P_{\Phi, \gamma}(\phi, \cdot) = \mathbb{Q}_{\phi(T)}(\cdot; \gamma),$$

for its transition kernel. If π_γ is the unique stationary distribution of X , this kernel admits $\mathbb{Q}_{\pi_\gamma}(\cdot; \gamma)$ as its stationary distribution.

We hope to use minorisation condition (4.1) to extend the state space Ω to a new space $\check{\Omega} = \Omega \times \{0, 1\}$, such that the Markov chain $(\Phi_n, Y_n)_{n \in \mathbb{N}}$ on $\check{\Omega}$ possesses an ergodic atom whilst retaining the marginal transition probabilities of the Φ component as given in Equation (4.5).

Mimicking the split chain constructions from [4] or [26, Section 17.3], we start by considering the T -skeleton chain for the original process $\{X_{nT}\}_{n \in \mathbb{N}}$. Given the minorisation (4.1), we can define $Y_n \in \{0, 1\}$, and obtain a Markov chain $\{(X_{nT}, Y_n)\}_{n \in \mathbb{N}}$ with associated probability measure $\check{\mathbb{P}}_\gamma$ by setting:

$$(4.7) \quad \begin{aligned} \check{\mathbb{P}}_\gamma(X_{(n+1)T} \in A | Y_n = 1, X_{nT}) &= \nu(A), \\ \check{\mathbb{P}}_\gamma(X_{(n+1)T} \in A | Y_n = 0, X_{nT}) &= \eta_\gamma(X_{nT}, A), \end{aligned}$$

where

$$(4.8) \quad \eta_\gamma(x, A) = \frac{P_\gamma^T(x, A) - \epsilon \nu(A)}{1 - \epsilon},$$

as well as:

$$(4.9) \quad \check{\mathbb{P}}_\gamma(Y_n = 1 | X_{nT}) = \epsilon.$$

It is a standard result that this chain has the correct marginal distributions for $\{X_{nT}\}_{n \in \mathbb{N}}$, and that the set $\chi \times \{1\}$ is a regenerative atom for the chain, i.e. $A \subset \chi, i \in \{0, 1\}$:

$$(4.10) \quad \check{\mathbb{P}}_\gamma(X_{(n+1)T} \in A, Y_{n+1} = i | X_{nT}, Y_n = 1) = \nu(A) \epsilon^i (1 - \epsilon)^{1-i}.$$

In other words, conditionally on $\{Y_n = 1\}$, the processes $\{X_{kT}, Y_k\}_{k \geq n+1}$ and $\{X_{kT}, Y_k\}_{k \leq n}$ are independent.

To transfer these properties over to the segment chain Φ , we bridge the paths from X_{nT} to $X_{(n+1)T}$ conditionally on the endpoints. We define the Radon-Nykodym derivatives $\frac{d\nu}{dP_\gamma^T}$ and $\frac{d\eta_\gamma}{dP_\gamma^T}$, which are functions of x and x' , and extend the measure $\check{\mathbb{P}}_\gamma$ to be a transition kernel from Φ_n to Φ_{n+1} . For the Y_n updates, we get:

$$(4.11) \quad \check{\mathbb{P}}_\gamma(Y_n = 1 | \{\Phi_k\}_{k=0}^n, \{Y_k\}_{k=0}^{n-1}) = \epsilon,$$

and for the Φ_{n+1} updates, we get:

$$(4.12) \quad \begin{aligned} \check{\mathbb{P}}_\gamma(\Phi_{n+1} \in A | Y_n = 1, \Phi_n) &= \int_A \frac{d\nu}{dP_\gamma^T}(\Phi_n(T), \phi(T)) d\mathbb{Q}_{\Phi_n(T)}(\phi; \gamma), \\ \check{\mathbb{P}}_\gamma(\Phi_{n+1} \in A | Y_n = 0, \Phi_n) &= \int_A \frac{d\eta_\gamma}{dP_\gamma^T}(\Phi_n(T), \phi(T)) d\mathbb{Q}_{\Phi_n(T)}(\phi; \gamma). \end{aligned}$$

One can check that these give the appropriate marginal transition kernels to recover $\Phi_{n+1} \sim \mathbb{Q}_{\Phi_n(T)}(\cdot; \gamma)$, and that $\Phi_{n+1}(T) | \Phi_n, \{Y = 1\} \sim \nu$. It is easy to check that the invariant distribution for the split segment chain is:

$$(4.13) \quad \check{\pi}_\gamma(A \times \{i\}) = \epsilon^i (1 - \epsilon)^{1-i} \mathbb{Q}_{\pi_\gamma}(A; \gamma),$$

for $A \in \mathcal{B}(\Omega)$.

Let $\check{P}_\gamma((\phi, y), \cdot)$ be the transition kernel of the split segment chain $\{\Phi_n, Y_n\}_{n \in \mathbb{N}}$, as given by Equations (4.11) and (4.12). Since $Y_n = 1$ implies that $X_{(n+1)T} \sim \nu$ independently of the history of the process up to time Tn , we can show that the split segment chain admits $\check{\alpha} = \Omega \times \{1\}$ as an atom:

LEMMA 4.4 (Atom for the Split Segment Chain). *For $\{\Phi_n, Y_n\}_{n \in \mathbb{N}}$ the split segment chain with transition law \check{P}_γ , we have that $\forall \phi \in \Omega$, and $\forall A \in \mathcal{B}(\Omega)$, $i \in \{0, 1\}$:*

$$\check{P}_\gamma^2((\phi, 1), A \times \{i\}) = C^i(1 - C)^{1-i} \mathbb{Q}_\nu(A; \gamma).$$

In particular, conditionally on the event $\{Y_n = 1\}$, the pre- n process $\{\Phi_k, Y_k\}_{k \leq n}$ and the post- $(n+2)$ process $\{\Phi_k, Y_k\}_{k \geq n+2}$ are independent. Given $\{Y_n = 1\}$, $\{\Phi_k, Y_k\}_{k \geq n+2}$ has the same law as $\{\Phi_k, Y_k\}_{k \geq 1}$ with initial distributions $\Phi_0(T) \sim \nu$ and $Y_0 \sim \text{Bern}(C)$.

With Lemma 4.4, we can consider an excursion process between hitting times of the atom $\check{\alpha}$, the details of which can be found in Appendix A.1. These are identically distributed, 1-dependent sequences of random ($\text{Geom}(\epsilon)$ distributed) length. This structure can be visualised in Figure 8.

As a follow-up remark, since $Y_n = 1$ implies that Φ_n and Φ_{n+2} are independent, we note that the “bridge” path Φ_{n+1} has the property that $\Phi_{n+1}(0) = \Phi_n(T)$ and $\Phi_{n+1}(T) = \Phi_{n+2}(0)$ are independent.

With this framework, any uniformly ergodic Markov process can be transformed into a discrete-time chain with an ergodic atom.

4.4. *Proving the Asymptotic Results.* We now have enough setup to prove the results in Theorem 3.5. Consider a bounded function $f : \mathbb{R}^d \rightarrow \mathbb{R}$, with $|f| \leq M$, and assume that $\pi_\gamma f = 0$ for all $\gamma \in \Gamma$. We are interested in the behaviour of the estimator \hat{f}_t as given in Equation (3.6). If the original process X is a continuous-time process, we write:

$$(4.14) \quad F(\phi) = \frac{1}{T} \int_{s=0}^T f(x_s) ds,$$

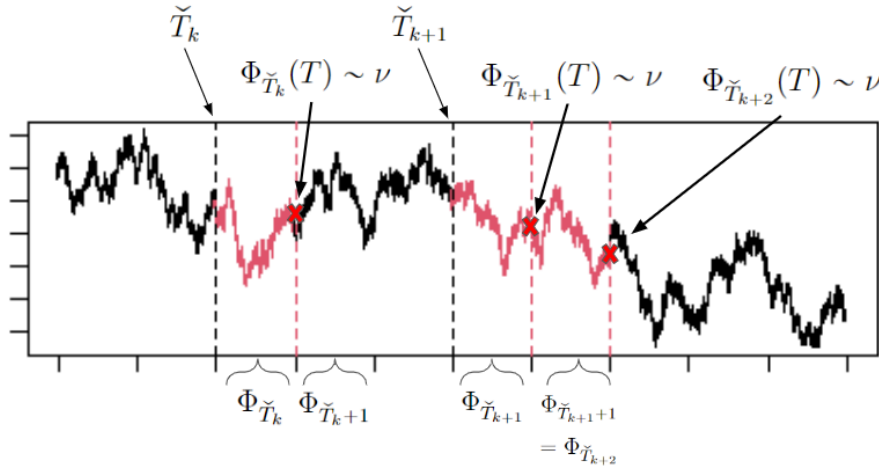


Fig 8: Example path including excursions (path is for illustration purposes and does not reflect a real sampling scheme). The regeneration times \check{T}_k (defined in appendix A.1) are shown, along with associated random variables: the regeneration segments $\Phi_{\check{T}_k}$ are shown in red. These segments are independent of neither the immediate past, nor the immediate future. The random length excursions Ψ_k go between red crosses and are identically distributed and 1-dependent.

for $\phi = \{x_s\}_{s=0}^T \in \Omega$, to get that:

$$(4.15) \quad \hat{f}_t = \frac{1}{n} \sum_{i=0}^{n-1} F(\Phi_i) + \mathcal{O}(t^{-1}),$$

where $n = \lfloor \frac{t}{T} \rfloor$. An analogous statement can be made for discrete-time processes. The asymptotic properties of \hat{f}_t will therefore be the same as those of:

$$(4.16) \quad \hat{f}_n^\Phi = \frac{1}{n} \sum_{i=0}^{n-1} F(\Phi_i),$$

as $n \rightarrow +\infty$.

Recall that we will be working with an AIR MCMC scheme where the lags between adaptation times are polynomially increasing. Let $\beta > 0, c \geq 1$ such that $\forall k \in \mathbb{N}$:

$$(4.17) \quad \frac{1}{c} k^\beta \leq n_k \leq c k^\beta,$$

for $n_k \in \mathbb{N}$. The adaptation times are then given by $N_k = \sum_{i=1}^k n_k$, with $N_0 = n_0 = 0$ for consistency of notation.

We consider the AIR segment chain process as follows: let $\{(\Phi_n, Y_n)\}_{n \in \mathbb{N}}$ evolve according to \tilde{P}_{γ_k} for $N_k \leq n < N_{k+1}$, then update the parameter to γ_{k+1} at N_{k+1} . In this setting, we obtain the following results:

THEOREM 4.5 (AIR Segment Chain \mathcal{L}^2 Convergence and CLT). *Consider $(\Phi_n, Y_n)_{n \geq 0}$ the AIR segment chain process, where the original family of transition kernels $\{P_\gamma\}_{\gamma \in \Gamma}$ have invariant distributions π_γ and satisfy the minorisation condition (4.1). Assume that f is bounded and $\mathbb{E}_{\pi_\gamma}(f(X)) = 0$ for all $\gamma \in \Gamma$. Then $\forall (\Phi_0, Y_0) \in \tilde{\Omega}$, $\gamma_0 \in \Gamma$, and any adaptation scheme:*

- For any $\beta > 0$, and $\forall \epsilon < \min\left(\frac{1}{2}, \frac{\beta}{1+\beta}\right)$,

$$n^\epsilon \hat{f}_n^\Phi \xrightarrow{\mathcal{L}^2} 0, \quad \text{as } n \rightarrow \infty.$$

- For $\beta > 1$, if $\gamma_i \xrightarrow{P} \gamma_\infty$ such that $\sigma^2(\gamma_\infty) > 0$, and that $\sigma^2(\gamma)$ is a continuous function of γ , then a CLT holds:

$$\sqrt{n} \hat{f}_n^\Phi \xrightarrow{D} \mathcal{N}(0, \sigma^2(\gamma_\infty)).$$

The proof of Theorem 4.5 is in appendix B.

We can also apply the almost sure convergence results from [23] to obtain almost sure convergence results:

THEOREM 4.6 (AIR Segment Chain Almost Sure Convergence). *Consider $(\Phi_n, Y_n)_{n \geq 0}$ the AIR segment chain process, where the original family of transition kernels $\{P_\gamma\}_{\gamma \in \Gamma}$ have invariant distributions π_γ and satisfy the minorisation condition (4.1). Assume that f is bounded and $\mathbb{E}_{\pi_\gamma}(f(X)) = 0$ for all $\gamma \in \Gamma$. Then $\forall (\Phi_0, Y_0) \in \tilde{\Omega}$, $\gamma_0 \in \Gamma$, and any adaptation scheme, if $\epsilon < \min\left(\frac{1}{2}, \frac{\beta}{1+\beta}\right)$ then:*

$$n^\epsilon \hat{f}_n^\Phi \xrightarrow{a.s.} 0.$$

This result follows directly from Theorems 4.3 and 4.5 of [23].

Finally, since $\hat{f}_t = \hat{f}_n^\Phi + \mathcal{O}(t^{-1})$, we can use Theorem 4.5 and Theorem 4.6 to immediately obtain the results on \hat{f}_t in Theorem 3.5, which concludes our discussion of the asymptotic results for the adaptive stereographic MCMC algorithms.

5. Simulation Studies. In this final section, we demonstrate the ability of our algorithms to perform well in challenging heavy-tailed, high-dimensional settings.

All code was run in Julia. We simulate the SBPS bounce events by combining the techniques from [13] and [1], with the use of the ForwardDiff package from [29]. We use the adaptive window width from [1], as it allows for significant flexibility in cases where the density may be highly concentrated, but we use Brent’s method from [13], rather than any methods involving Hessian information, since Hessian matrices can be very expensive in high dimensions.

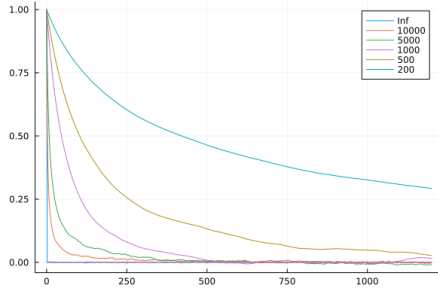
5.1. Impact of Parameters on Mixing. We present a comparison of autocorrelation plots targeting a MtD in d dimensions with d DoF. We compare the autocorrelation of $\|X\|^2$ for $d = 100$ when taking γ to be based on the mean and covariance of n iid $\mathcal{N}(0_d, I_d)$ random vectors, reflecting what we might expect in at different stages of a run of our AIR algorithms. As n increases, the parameter estimators converge to the optimal parameters, which leads to π_γ becoming uniform over \mathbb{S}^d . We start all algorithms in stationarity and do not perform adaptations to demonstrate the improved performance we obtain by updating the parameter estimates. For the SRW and SBPS respectively, we tune h and λ_{ref} following the intuition given in the closing remarks of Section 3.1.

In all cases, we see from Figure 9 that the autocorrelation dramatically improves as n increases. In the optimal $n = \infty$ case, we see that the SRW and SSS achieve essentially uncorrelated moves after only one step (in fact, the SSS is obtaining truly independent samples after only one step). For the SBPS, we can observe the strength of the non-reversible dynamics in producing negatively correlated samples in the optimal setting. This clearly demonstrates the benefit of using adaptive methods to improve γ , since it yields such large improvements in autocorrelation.

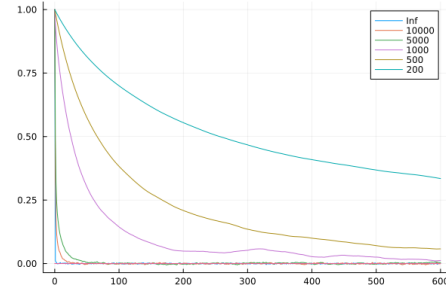
When comparing the deterioration of the different algorithm as n decreases, the SSS performs better than the SRW, since its autocorrelations decay more slowly. For the SBPS, the case $n = \infty$ seems very promising, but once the spherical symmetry is even slightly lost then it begins to perform the worst out of all the algorithms. It is also worth noting that, in the optimal setting, the SBPS is significantly more expensive than either of the other two algorithms. For every 1 unit time of SBPS sample path, we could simulate roughly 200 steps of SRW or SSS. The SRW and SSS have comparable computational costs in the optimal regime, but the cost of one step of SRW does not increase as the quality of the parameters decreases. On the other hand, tuning the step size h of the SRW can be challenging, whereas the SSS has no similar parametrisation issues.

5.2. Robustness of Adaptive Algorithms. Having looked at the improvements that adaptations can bring when sampling from stationarity, we now demonstrate the robustness of the adaptive algorithms to starting deep in the tails of the target with poor initial parameters. Consider targeting a MtD with $\nu = 2$, $d = 200$, which is far beyond the theoretical assumptions for Theorem 3.5 to guarantee convergence of estimators. We set the initial parameters $\mu = (1000, \dots, 1000)$, $\Sigma = dI_d$, and start the process on the equator to emulate a situation where the prior and posterior modes are very far apart and the target is heavy-tailed.

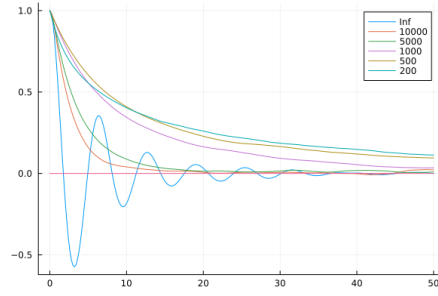
We present plots of the sample paths for the adaptive SRW, SSS, SBPS, and a plot of a HMC sample path struggling to find the modes for comparison. These are Figures 11, 12, 13,



(a) Autocorrelation for SRW



(b) Autocorrelation for SSS



(c) Autocorrelation for SBPS

Fig 9: Autocorrelation plots of $\|X\|^2$ for the stereographic algorithms targeting a MtD with $\nu = d = 100$. γ is taken as the empirical mean and covariance estimator for n iid $\mathcal{N}(0_d, I_d)$ with n varying from 200 to ∞ .

and 10 respectively. We also include plots of the number of likelihood evaluations per step for the SSS and number of gradient evaluations per unit time for the SBPS to show how the computational cost of the algorithms changes with the adaptations.

For our adaptation scheme, we use the latest quarter of the adaptive epochs to obtain an estimator for the target mean and covariance matrix via the standard empirical estimators. We also scale the covariance matrix to center the latest adaptive epoch's sample path around the equator. This scaling is included to force the probability mass onto the equator and control our estimators in cases where the target covariance may be infinite.

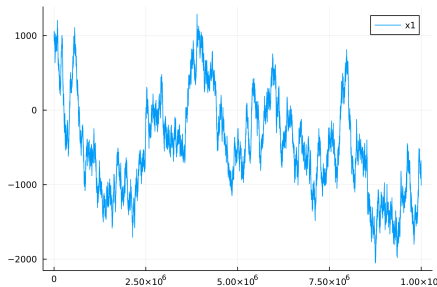
(a) Plot of the first coordinate X_1 (b) Plot of the norm $\|X\|$

Fig 10: HMC sample paths targeting a MtD with $\nu = 2$, $d = 200$, started at $x_0 = (1000, \dots, 1000)$. This run took approximately 3.5 hours.

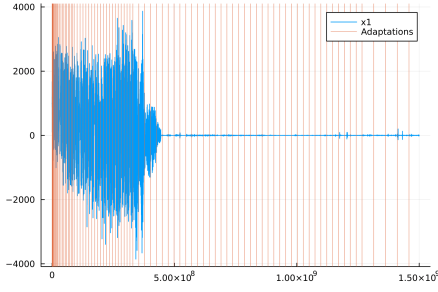
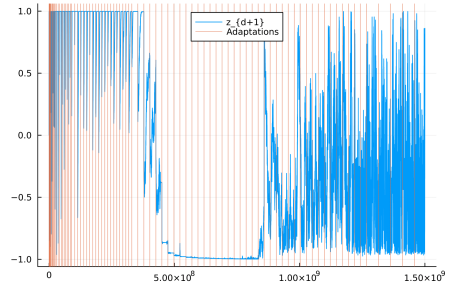
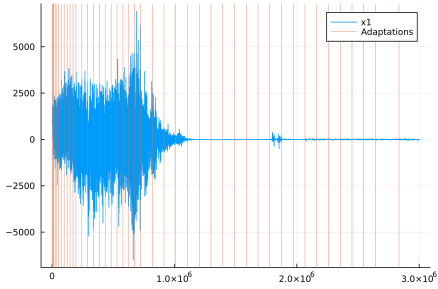
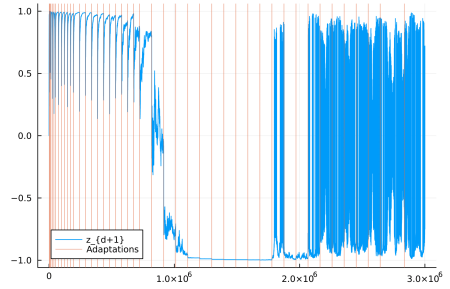
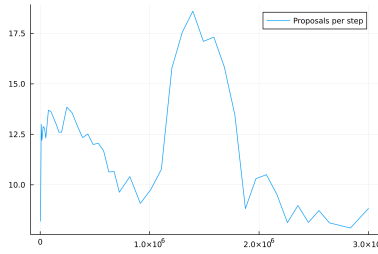
(a) Plot of the first coordinate X_1 (b) Plot of the latitude Z_{d+1}

Fig 11: Adaptive SRW sample paths targeting a MtD with $\nu = 2$, $d = 200$, and initial parameters $\mu = (1000, \dots, 1000)$, $\Sigma = dI_d$. We adaptively tune h to target an average acceptance probability of 23.4%. This run took approximately 6 hours and 20 minutes.

(a) Plot of the first coordinate X_1 (b) Plot of the latitude Z_{d+1} 

(c) Average number of proposals per step over the run of the SSS

Fig 12: Adaptive SSS sample paths targeting a MtD with $\nu = 2$, $d = 200$, and initial parameters $\mu = (1000, \dots, 1000)$, $\Sigma = dI_d$. This run took approximately 15 minutes.

The HMC sample path in Figure 10 was essentially unable to make any progress in finding the mode of the target distribution. This is to be expected when the tails of the distribution are so heavy and the dimension is relatively large.

The first thing the stereographic algorithms do in every case is to gradually make their way towards N , then expand the radius of the sphere through the adaptation scheme, then continue going towards N (this can be seen by the plots of the trajectories of Z_{d+1} in Figures 11b, 12b and 13b). In the X_1 path, this exploration leads to widening oscillations more or less symmetrically around the initial parameter μ .

The algorithms then take varying lengths of time to find the true mean of the target distribution. The SBPS takes longer to expand the sphere, but then finds the mean very quickly, as

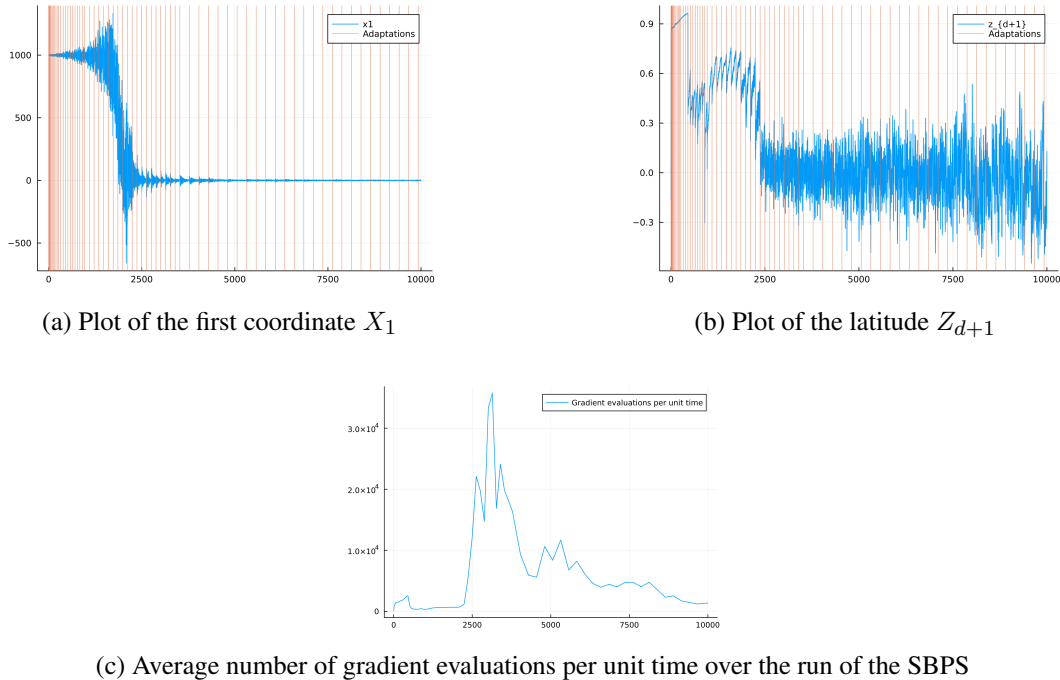


Fig 13: Adaptive SBPS sample paths targeting a MtD with $\nu = 2$, $d = 200$, and initial parameters $\mu = (1000, \dots, 1000)$, $\Sigma = dI_d$. We set $\lambda_{\text{ref}} = 1$ throughout. This run took approximately 1 hour 40 minutes.

seen in Figure 13a. The SRW or SSS both expand the radius very quickly, then require more algorithm time to find the mean, as in Figure 11a or 12a.

From there, the behaviour of the algorithms is slightly different. For the SRW and SSS, once the mean is found, they are able to stay there and adapt the μ parameter to recenter the sphere around the true mean. The process in then drops down from the North pole, but may now need a long time to shrink the Σ parameter back down to match the target, leading to a long time stuck at the South pole. This is clearly seen in the plots of Z_{d+1} in Figure 11b or 12b.

For the SBPS, the latitude plot appears to suggest it skips this portion of the adaptations and immediately moves the mass onto the equator. However, it transpires that the algorithm may have successfully put the probability mass around $Z_{d+1} \approx 0$, but it had actually focused the target density onto a small corner of the equator: as the adaptations move μ from $(1000, \dots, 1000)$ to 0_d , Σ scales itself so that the probability mass becomes isolated onto a small subset of the equator. It takes a long time for the process to fully learn μ , at which point Σ can be updated to spread the probability mass evenly around the equator.

Since the estimators for the sample mean and covariance are still trying to balance a large number of points near $(1000, \dots, 1000)$ with the incoming samples near 0_d , the estimators for Σ become temporarily highly heterogeneous. This results in a spike in the computational cost of the SBPS just after the process gets near the true mode, as shown in Figure 13c. A similar spike is present for the SSS, as seen in Figure 12c, but the computational cost only goes up by a factor of 2, not the factor of 30 seen in the SBPS. This once again highlights the computational cost of the SBPS when compared with the other algorithms, which was also seen to be a problem in the stationary regime in Section 5.1.

Both of our simulation studies so far suggest that the SSS will outperform both the SRW and SBPS, partly because it is able to perform efficient global moves without the need for

extra parametrisation, but also because it is very cheap to simulate: the overall runtime of the SSS was 15 minutes, as opposed to 1 hour 40 minutes for the SBPS or 6 hours 20 minutes for the SRW. For this reason, we currently recommend using the SSS over either of the other two algorithms.

However, these plots also suggest that the uninformed proposals in the SSS cause it to struggle to find the mode, whereas the SBPS is able to do so very quickly once it reaches the appropriate latitude. We therefore expect that certain scenarios must exist in which the SBPS’s gradient based dynamics allow it to outperform the SSS, though we are yet to find a setting in which this overcomes the computational cost attached to the SBPS.

6. Discussion. We have discussed the use of adaptive MCMC methods to automatically tune the parameters of our stereographic algorithms. The theoretical results also provide insight into other potential uniformly ergodic algorithms: the segment chain framework can be used going forward to prove convergence results for any adaptive MCMC algorithm based on a simultaneously uniformly ergodic collection of Markov kernels, particularly in the continuous-time setting. This addresses a gap in the current literature, where the focus has predominantly been on discrete-time algorithms.

Alongside theoretical convergence results, we have demonstrated our algorithms’ ability to adapt to the target distribution and improve sampling efficiency in problems far more challenging than those covered by the theorems. These examples highlight the power of the stereographic projection as a way of helping sample from heavy-tailed distributions, since standard off-the-shelf methods (namely HMC) have great difficulty tackling these problems when they find themselves in the tails.

All three stereographic algorithms are able to target high-dimensional, heavy-tailed target distributions, and we demonstrated their ability to tune parameters when started in the tails. In terms of their relative mixing properties in the stationary regime, we see that the SSS performs best of the three algorithms. The SBPS is too computationally expensive to compete with it, whereas the SRW is not as robust as the SSS, requires extra tuning, and cannot as easily do global jumps outside of the perfect setting.

We conclude this paper with several further avenues of research:

SBPS Refreshment Rate: Several results exist discussing the behaviour of the Euclidean BPS algorithm as one varies the refreshment rate λ_{ref} [6, 8]. It would be of interest to analyse the SBPS using similar methods to better understand the implications of choices of λ_{ref} on the mixing properties of the algorithm.

Other Stereographic Algorithms: We have seen that the stereographic projection naturally leads to uniformly ergodic algorithms, even when the target distribution is heavy-tailed. It is therefore natural to consider stereographic versions of other commonly used algorithms, namely MALA or HMC, potentially following the works of [19] on targeting distributions defined on Riemannian manifolds. However, early attempts at constructing these proposals lead to many cases where the proposed moves “fall off the sphere” and must be rejected, indicating similar issues to cases where these algorithms have been used to target light-tailed distributions in Euclidean space. Table 1 of [14] gives a good summary of these points.

Generalising the Segment Chain: Though the segment chain is an elegant way of proving results when the underlying Markov kernels are uniformly ergodic, this is generally too strong an assumption. It is therefore of interest to see whether a segment chain framework could be used under weaker assumptions of geometric or polynomial ergodicity. Initial attempts at doing similar strategies have yielded issues with bounding the return times of the T-skeleton to the small set, since results such as those in [15] do not allow for bounds or constructions of small sets simultaneously over parameters.

More Simulation Studies: Finally, there is still much investigation required into the behaviour of the stereographic algorithms (adaptive or not) in cases where the target distributions are irregular. It would be of interest to do a more thorough overview of how the stereographic projection improves MCMC related analysis in real world applications where heavy-tailed distributions arise. We also have yet to find a case in which the SSS shows any reasonable flaw when compared to the other algorithms.

APPENDIX A: FURTHER DETAILS

A.1. Excursions of the segment chain. We discuss the regenerations and excursions of the split segment chain $\{(\Phi_n, Y_n)\}_{n \in \mathbb{N}}$.

We will write ν^* for an arbitrary measure on $\check{\Omega}$ such that, for $A \in \mathcal{B}(\mathbb{R}^d \times \mathbb{S}^{d-1})$ and $i = 0, 1$:

$$(A.1) \quad \nu^*(\phi(T) \in A, Y = i) = \epsilon^i (1 - \epsilon)^{1-i} \nu(A),$$

i.e., such that $\Phi \sim \nu^* \implies \Phi(T) \sim \nu$ and $Y \sim \text{Bern}(\epsilon)$.

Since the Y_n updates are not affected by the current position Φ_n , we can very easily identify the behaviour of our regeneration times. For $k \geq 1$, the hitting and return times of the atom are:

$$(A.2) \quad \begin{aligned} \check{\sigma}_1 &= \inf(n \geq 0 : Y_n = 1), & \check{\sigma}_k &= \inf(n > \check{\sigma}_{k-1} : Y_n = 1), \\ \check{\tau}_1 &= \inf(n \geq 1 : Y_n = 1), & \check{\tau}_k &= \inf(n > \check{\tau}_{k-1} : Y_n = 1). \end{aligned}$$

Alongside Lemma 4.4, we can concisely write that $\{\Phi_l, Y_l\}_{l \geq \check{\sigma}_k+2}$ has the same law as $\{\Phi_k, Y_k\}_{k \geq 1}$ started from $(\Phi_0, Y_0) \sim \nu^*$.

Thanks to uniform ergodicity, we can obtain the following explicit result on the distribution of the delayed renewal sequence $\{\check{\sigma}_k\}_{k \in \mathbb{N}}$.

LEMMA A.1 (Return Times to the Atom). *For $\{\Phi_n, Y_n\}_{n \in \mathbb{N}}$ the split segment chain with transition law \check{P}_γ , let $\{\check{\sigma}_k\}_{k \in \mathbb{N}}$ be as given in Equation (A.2). Then the inter-arrival times $\check{\sigma}_{n+1} - \check{\sigma}_n$ for $n \geq 1$ are iid $\text{Geom}(\epsilon)$ random variables.*

Note in particular that since ϵ does not depend on γ , neither does the distribution of the inter-arrival times.

Finally, we can define the notion of excursions from the atom, allowing us to divide sample paths into 1-dependent, identically distributed blocks. It is convenient to define the regeneration times:

$$(A.3) \quad \check{T}_k = \check{\sigma}_k + 1,$$

such that $\Phi_{\check{T}_k}(T) \sim \nu$ independently of $\{\Phi_n\}_{n \leq \check{\sigma}_k}$ (and also of $\Phi_{\check{T}_k}(0) = \Phi_{\check{\sigma}_k}(T)$), and so $\Phi_{\check{T}_{k+1}} \sim \mathbb{Q}_\nu(\cdot; \gamma)$ independently of the pre- $\check{\sigma}_k$ process, as in Lemma 4.4.

For $k \geq 0$, we define the excursion paths:

$$(A.4) \quad \Psi_k = \{\Phi_n, Y_n\}_{n=\check{T}_k+1}^{\check{T}_{k+1}},$$

These are random sequences in Ω of a.s. finite length, starting from $\Phi_{\check{T}_{k+1}}(0) = \Phi_{\check{T}_k}(T) \sim \nu$, and ending with $\Phi_{\check{T}_{k+1}}(T) \sim \nu$. By the above discussion, we can see that the variables $\{\Psi_k\}_{k \in \mathbb{N}}$ are identically distributed and 1-dependent. See Figure 8 for a visualisation of how \check{T}_k , Φ_n , ν , and Ψ_k all fit together.

We can use [4, Lemma 5.2], alongside the minorisation condition (4.1), to find the distribution of $\Phi_{\check{\sigma}_k}(T)$.

LEMMA A.2 (Stationarity at Renewal Times). *For ν and η_γ as defined in Equation (4.1) and Equation (4.8), we have that the unique stationary distribution π_γ of the original process X is given by:*

$$\pi_\gamma(\cdot) = \epsilon \sum_{n=1}^{\infty} (1 - \epsilon)^n \nu \eta_\gamma^{n-1}(\cdot).$$

As an immediate consequence, we get that $\Phi_{\check{\sigma}_k}(T) \sim \pi_\gamma$, for every $k \geq 2$.

The first statement is exactly Lemma 5.2 from [4], but with our notation. The distribution of $\Phi_{\check{\sigma}_k}(T)$ then follows from the geometric distribution of $\check{\sigma}_k - \check{\sigma}_{k-1}$.

A.2. Assumptions on the Adaptation Times. Recall that in assumption 3.2, we included “mild conditions” on the adaptation lags t_k . These additional conditions arise via the construction of the segment chain $\{\Phi_n\}_{n \in \mathbb{N}}$ featuring in our proofs. Since we wish to run the AIR framework on the discrete-time Markov process formed of segments of length T , it follows that we must adapt at integer multiples of T , so that $t_k = T \times n_k$.

Thus, we see that we will require the lags in Theorem 3.5 to have a common divisor, at least for large k . This condition can be difficult to satisfy if T is unknown, as is the case for the SBPS. Fortunately, since the minorisation condition (4.1) still holds if you increase T , we can consider a sequence of lags t_k such that $\lim_{k \rightarrow \infty} (\gcd(\{t_j : j \geq k\})) = \infty$, such as:

$$(A.5) \quad t_k = \inf(2^n : 2^n \geq k^\beta).$$

One can check that $t_k = \Theta(k^\beta)$, whilst having increasingly large common divisors. We can then apply the segment chain results once $t_k \geq T$, and consider the first part of the chain as asymptotically irrelevant.

APPENDIX B: PROOF OF THEOREM 4.5

In this section, we prove our main result, Theorem 4.5. We do this by bringing together the 1-dependent, identically distributed excursions Ψ_k discussed in Appendix A.1 and control the variance of our estimators.

For $i \in \mathbb{N}$, we define the Markov chain $\{H_j^{(i)}\}_{j \in \mathbb{N}}$ to have transition kernel \check{P}_{γ_i} , such that:

$$(B.1) \quad H_j^{(i)} = (\Phi_{N_i+j}, Y_{N_i+j}),$$

for $j = 0, \dots, n_{i+1} - 1$, and $H_j^{(i)}$ evolves independently of $\{(\Phi_n, Y_n)\}_{n \geq N_{i+1}}$ for $j \geq n_{i+1}$.

As in [12, Section 7], we let:

$$(B.2) \quad s_i = \sum_{j=N_i}^{N_{i+1}-1} F(\Phi_j) = \sum_{j=0}^{n_{i+1}-1} F(H_j^{(i)}),$$

where we abuse notation slightly and set $F(\phi, y) = F(\phi)$. Next, we let:

$$(B.3) \quad \sigma_1^{(i)} = \inf(j \geq 0 : H_j^{(i)} \in \check{\alpha}), \quad \sigma_{k+1}^{(i)} = \inf(j > \sigma_k^{(i)} : H_j^{(i)} \in \check{\alpha}),$$

$$T_k^{(i)} = \sigma_k^{(i)} + 1,$$

for $k \geq 1$ be the regeneration times for the $H^{(i)}$ process, defined analogously to \check{T}_k in (A.3). We can therefore write these excursions as:

$$(B.4) \quad \Psi_j^{(i)} = \{H_n^{(i)}\}_{n=T_j^{(i)}+1}^{T_{j+1}^{(i)}}.$$

By Lemma 4.4, these excursions are identically distributed for i fixed and, conditionally on γ_i , they are 1-dependent.

We also define:

$$(B.5) \quad L_i = \inf(l \geq 1 : T_l^{(i)} \geq n_{i+1} - 1) = 1 + \sum_{j=0}^{n_{i+1}-2} \mathbb{1}(H_j^{(i)} \in \check{\alpha}),$$

such that the last excursion of $H^{(i)}$ to start before we decouple from (Φ, Y) ends at step $T_{L_i}^{(i)}$.

Finally, we can define the sums over excursions which we will be analysing:

$$(B.6) \quad \begin{aligned} \eta_i &= \sum_{j=0}^{T_1^{(i)}} F(H_j^{(i)}), & \xi_i &= \sum_{j=T_1^{(i)}+1}^{T_{L_i}^{(i)}} F(H_j^{(i)}) \\ \zeta_i &= \sum_{j=n_{i+1}}^{T_{L_i}^{(i)}} F(H_j^{(i)}), & \xi_{i,j} &= \sum_{m=T_j^{(i)}+1}^{T_{j+1}^{(i)}} F(H_m^{(i)}). \end{aligned}$$

For fixed i , since $\xi_{i,j}$ are functions of $\Psi_j^{(i)}$ only, these are identically distributed, 1-dependent (conditionally on γ_i) random variables.

With these, we get that:

$$(B.7) \quad s_i = \sum_{j=N_i}^{N_{i+1}-1} F(\Phi_j) = \eta_i + \xi_i - \zeta_i.$$

η_i is a function of the $H^{(i)}$ path up until the first regeneration, and ζ_i is a function of the $H^{(i)}$ path from the point where we decouple from (Φ, Y) to the next regeneration. For large i , the vast majority of the sample path will be within the ξ_i term. The majority of the asymptotic results will then follow by studying $\xi_i = \sum_{j=1}^{L_i-1} \xi_{i,j}$, with $\xi_{i,j}$ identically distributed, conditionally 1-dependent random variables.

For the empirical sums $S_N = \sum_{j=0}^{N-1} F(\Phi_j)$, we can find $k = k(N)$ such that $N_k \leq N < N_{k+1}$ and write:

$$(B.8) \quad \begin{aligned} S_N &= \sum_{i=0}^k s_i + \sum_{j=N_k}^{N-1} F(\Phi_j) \\ &= \sum_{i=0}^{k-1} \eta_i + \sum_{i=0}^{k-1} \xi_i - \sum_{i=0}^{k-1} \zeta_i + \sum_{j=N_k}^{N-1} F(\Phi_j), \\ &= \Xi_k^{(1)} + \Xi_k^{(2)} + \Xi_k^{(3)} + \Xi_{k,N}^{(4)}. \end{aligned}$$

Since our estimator of interest is $\hat{f}_n^\Phi = \frac{1}{n} S_n$, it only remains to study the asymptotic behaviour of $\Xi_k^{(m)}$, $m \in \{1, 2, 3\}$, and $\Xi_{k,N}^{(4)}$ as N becomes large and the adaptive parameter γ_i varies.

We follow the steps of the proofs found in [12, Section 7]. Our scenario has the advantage that, since our original minorisation condition (4.1) was uniform over the sample space, our ergodic atom has geometric return times. However, we have the difficulty that our (Φ, Y) regenerations are 2-step regenerations, rather than 1-step regenerations, which means that our excursions are 1-dependent, not independent.

We write expectations of the form $\mathbb{E}_{(\phi,y)}^{\gamma_0}$ as expectations with initial value (ϕ, y) and initial adaptive parameter γ_0 . If integrands are independent of the initial values (Φ_0, Y_0) , we shall simply write \mathbb{E}^γ . The underlying adaptation scheme which updates γ_k is then assumed to be included in the relevant expectations.

B.1. Asymptotic Behaviour of $\Xi_k^{(2)}$. Since most of the sample path will be contained in the $\Xi_k^{(2)}$ term, we start by studying its properties. The other terms can be controlled relatively easily thanks to the boundedness of f and the geometric tails of distribution of the excursion lengths.

We define the asymptotic variance function as:

$$(B.9) \quad \sigma^2(\gamma) = \epsilon \mathbb{E}^\gamma(\xi_{1,1}^2) + 2\epsilon \mathbb{E}^\gamma(\xi_{1,1}\xi_{1,2})$$

not to be confused with the stopping times $\sigma_j^{(i)}$. We have that:

$$(B.10) \quad \begin{aligned} \mathbb{E}^\gamma(\xi_{1,1}^2) &= \mathbb{E}^\gamma\left(\left[\sum_{m=\tilde{T}_1+1}^{\tilde{T}_2} F(\Phi_m)\right]^2\right) = \mathbb{E}^\gamma\left(\left[\sum_{m=\tilde{\tau}_1+2}^{\tilde{\tau}_2+1} F(\Phi_m)\right]^2\right) \\ &= \mathbb{E}_{\nu^*}^\gamma\left(\left[\sum_{m=1}^{\tilde{\sigma}_1+1} F(\Phi_m)\right]^2\right), \end{aligned}$$

so since f is bounded and $\tilde{\sigma}_1 \sim \text{Geom}(\epsilon)$, we can use the Cauchy-Schwartz inequality to get:

$$(B.11) \quad \sup_{\gamma \in \Gamma} \sigma^2(\gamma) < \infty.$$

We start by giving explicit expressions for the moments of ξ_i :

LEMMA B.1 (Moments of ξ_i). *Consider $\xi_{i,j}$ and ξ_i as given in Equation (B.6). Then, if $\mathbb{E}_{\pi_\gamma}(f(X)) = 0$:*

$$\begin{aligned} \mathbb{E}^{\gamma_0}(\xi_{i,j}|\gamma_i) &= \mathbb{E}^{\gamma_0}(\xi_i|\gamma_i) = 0, \\ \mathbb{E}^{\gamma_0}(\xi_i^2|\gamma_i) &= (n_{i+1} - 1)\sigma^2(\gamma_i) - 2\mathbb{E}^{\gamma_i}(\xi_{1,1}\xi_{1,2}), \\ \mathbb{E}^{\gamma_0}(\xi_i^4|\gamma_i) &= \mathcal{O}(n_{i+1}^2), \end{aligned}$$

where the \mathcal{L}^4 bound holds uniformly over γ_i .

The first statement follows from standard relations between excursions and stationary measures. The second statement follows from Wald's identity. The third statement follows from a martingale argument using Doob's inequality.

PROOF OF LEMMA B.1. For $i \geq 0$ fixed, recall that $\xi_{i,j}$ are identically distributed random variables. We therefore have that:

$$\begin{aligned} \mathbb{E}^{\gamma_0}(\xi_{i,j}|\gamma_i) &= \mathbb{E}^{\gamma_0}\left(\sum_{m=T_j^{(i)}+1}^{T_{j+1}^{(i)}} F(H_m^{(i)}) \middle| \gamma_i\right) \\ &= \mathbb{E}^{\gamma_i}\left(\sum_{m=\tilde{T}_j+1}^{\tilde{T}_{j+1}} F(\Phi_m)\right), \end{aligned}$$

must be constant over j . By Theorem 10.0.1 of [26], we have that:

$$\mathbb{E}_{\tilde{\pi}_\gamma}^\gamma \left(\mathbb{1}(Y_0 = 1) \sum_{m=1}^{\tilde{\tau}_1} F(\Phi_m) \right) = \mathbb{E}_{\tilde{\pi}_\gamma}(F(\Phi)) = 0.$$

Writing $\tilde{\pi}|_{\tilde{\alpha}}(\cdot) = \epsilon^{-1} \tilde{\pi}_\gamma(\cdot \cap \{Y = 1\})$, we rewrite this as:

$$(B.12) \quad \mathbb{E}_{\tilde{\pi}|_{\tilde{\alpha}}}^\gamma \left(\sum_{m=1}^{\tilde{\tau}_1} F(\Phi_m) \right) = \epsilon^{-1} \mathbb{E}_{\tilde{\pi}_\gamma}^\gamma \left(\mathbb{1}(Y_0 = 1) \sum_{m=1}^{\tilde{\tau}_1} F(\Phi_m) \right) = 0.$$

Exactly as in Equation (B.10), for any initial distribution μ :

$$\mathbb{E}_\mu^\gamma \left(\sum_{m=\tilde{T}_j+1}^{\tilde{T}_{j+1}} F(\Phi_m) \right) = \mathbb{E}_{\nu^*}^\gamma \left(\sum_{m=1}^{\tilde{\sigma}_1+1} F(\Phi_m) \right).$$

Comparing this with Equation (B.12), we see that:

$$\begin{aligned} \mathbb{E}_{\nu^*}^\gamma \left(\sum_{m=1}^{\tilde{\sigma}_1+1} F(\Phi_m) \right) &= \mathbb{E}_{\tilde{\pi}|_{\tilde{\alpha}}}^\gamma \left(\sum_{m=\tilde{\sigma}_1+2}^{\tilde{\sigma}_2+1} F(\Phi_m) \right) \\ &= \mathbb{E}_{\tilde{\pi}|_{\tilde{\alpha}}}^\gamma \left(\sum_{m=1}^{\tilde{\tau}_1} F(\Phi_m) \right) + \mathbb{E}_{\tilde{\pi}|_{\tilde{\alpha}}}^\gamma (F(\Phi_{\tilde{\sigma}_2+1})) - \mathbb{E}_{\tilde{\pi}|_{\tilde{\alpha}}}^\gamma (F(\Phi_1)) \\ &= \mathbb{E}_{\tilde{\pi}|_{\tilde{\alpha}}}^\gamma (F(\Phi_{\tilde{T}_2})) - \mathbb{E}_{\tilde{\pi}|_{\tilde{\alpha}}}^\gamma (F(\Phi_1)). \end{aligned}$$

However, Lemma A.2 tells us that, given $\Phi_0(T) \sim \pi_\gamma$ and $Y_0 = 1$, we have that Φ_1 and $\Phi_{\tilde{T}_2}$ have the same distribution. Hence:

$$(B.13) \quad \mathbb{E}_{\nu^*}^\gamma \left(\sum_{m=1}^{\tilde{\sigma}_1+1} F(\Phi_m) \right) = 0 \quad \implies \quad \mathbb{E}^{\gamma_0}(\xi_{i,j}|\gamma_i) = 0.$$

For $\mathbb{E}^{\gamma_0}(\xi_i|\gamma_i) = \mathbb{E}^{\gamma_0}(\sum_{j=1}^{L_i-1} \xi_{i,j}|\gamma_i)$, we use Wald's identity. For this, we require that:

$$(B.14) \quad \mathbb{E}^{\gamma_0}(\xi_{i,j} \mathbb{1}(L_i - 1 \geq j)|\gamma_i) = \mathbb{E}^{\gamma_0}(\xi_{i,j}|\gamma_i) \mathbb{P}^{\gamma_0}(L_i - 1 \geq j),$$

for every j (recalling that $\sigma_j^{(i)}$ are independent of γ_i , so L_i is also).

However, $\{L_i - 1 \geq j\} = \{T_j^{(i)} < n_{i+1} - 1\} = \{\sigma_j^{(i)} \leq n_{i+1} - 3\}$. Since $\xi_{i,j}$ is a function of the excursion $\Psi_j^{(i)}$, it is independent of the event $\{\sigma_j^{(i)} \leq n_{i+1} - 3\}$, giving the required condition.

Thus, we can apply Wald's identity to get that:

$$(B.15) \quad \mathbb{E}^{\gamma_0}(\xi_i|\gamma_i) = \mathbb{E}^{\gamma_0} \left(\sum_{j=1}^{L_i-1} \xi_{i,j} \middle| \gamma_i \right) = \mathbb{E}^{\gamma_0}(L_i - 1) \times \mathbb{E}^{\gamma_0}(\xi_{i,1}|\gamma_i) = 0.$$

For $\mathbb{E}^{\gamma_0}(\xi_i^2|\gamma_i)$, we follow an argument similar to the standard proof of Wald's identity:

$$\mathbb{E}^{\gamma_0}(\xi_i^2|\gamma_i) = \mathbb{E}^{\gamma_0} \left(\left[\sum_{j=1}^{L_i-1} \xi_{i,j} \right]^2 \middle| \gamma_i \right)$$

$$\begin{aligned}
&= \mathbb{E}^{\gamma_0} \left(\left[\sum_{j=1}^{\infty} \xi_{i,j} \mathbb{1}(\sigma_j^{(i)} \leq n_{i+1} - 3) \right]^2 \middle| \gamma_i \right) \\
&= \sum_{j=1}^{\infty} \mathbb{E}^{\gamma_0} \left(\xi_{i,j}^2 \mathbb{1}(\sigma_j^{(i)} \leq n_{i+1} - 3) \middle| \gamma_i \right) \\
&\quad + 2 \sum_{j < k} \mathbb{E}^{\gamma_0} \left(\xi_{i,j} \xi_{i,k} \mathbb{1}(\sigma_j^{(i)} \leq n_{i+1} - 3) \mathbb{1}(\sigma_k^{(i)} \leq n_{i+1} - 3) \middle| \gamma_i \right) \\
&= \sum_{j=1}^{\infty} \mathbb{E}^{\gamma_0} \left(\xi_{i,j}^2 \mathbb{1}(\sigma_j^{(i)} \leq n_{i+1} - 3) \middle| \gamma_i \right) \\
&\quad + 2 \sum_{j < k} \mathbb{E}^{\gamma_0} \left(\xi_{i,j} \xi_{i,k} \mathbb{1}(\sigma_k^{(i)} \leq n_{i+1} - 3) \middle| \gamma_i \right),
\end{aligned}$$

since $j < k \implies \sigma_j^{(i)} < \sigma_k^{(i)}$. The first sum, using Wald's identity, can be simplified to:

$$(B.16) \quad \sum_{j=1}^{\infty} \mathbb{E}^{\gamma_0} \left(\xi_{i,j}^2 \mathbb{1}(\sigma_j^{(i)} \leq n_{i+1} - 3) \middle| \gamma_i \right) = \mathbb{E}^{\gamma_0}(L_i - 1) \times \mathbb{E}^{\gamma_0}(\xi_{i,1}^2 | \gamma_i).$$

For the second term, if we condition on the σ -algebra $\mathcal{F}_{T_{j+1}^{(i)}}$ and $k > j + 1$, then the 1-dependent structure of the excursions gives that $\xi_{i,k}$ is conditionally independent of $\xi_{i,j} \mathbb{1}(\sigma_k^{(i)} \leq n_{i+1} - 3)$ and these expectations must be 0. Thus:

$$(B.17) \quad \sum_{j < k} \mathbb{E}^{\gamma_0} \left(\xi_{i,j} \xi_{i,k} \mathbb{1}(\sigma_k^{(i)} \leq n_{i+1} - 3) \middle| \gamma_i \right) = \sum_{j=1}^{\infty} \mathbb{E}^{\gamma_0} \left(\xi_{i,j} \xi_{i,j+1} \mathbb{1}(\sigma_{j+1}^{(i)} \leq n_{i+1} - 3) \middle| \gamma_i \right).$$

Since $\xi_{i,j+1}$ is independent of $\{H_m^{(i)}\}_{m=0}^{\sigma_{j+1}^{(i)}}$ conditionally on γ_i , we have that:

$$\begin{aligned}
&\mathbb{E}^{\gamma_0} \left(\xi_{i,j} \xi_{i,j+1} \mathbb{1}(\sigma_{j+1}^{(i)} \leq n_{i+1} - 3) \middle| \gamma_i \right) \\
&= \mathbb{E}^{\gamma_0} \left(F(\Phi_{T_{j+1}^{(i)}}) \xi_{i,j+1} \mathbb{1}(\sigma_{j+1}^{(i)} \leq n_{i+1} - 3) \middle| \gamma_i \right) \\
&\quad + \mathbb{E}^{\gamma_0}(\xi_{i,j+1} | \gamma_i) \mathbb{E}^{\gamma_0} \left(\mathbb{1}(\sigma_{j+1}^{(i)} \leq n_{i+1} - 3) [\xi_{i,j} - F(\Phi_{T_{j+1}^{(i)}})] \middle| \gamma_i \right) \\
&= \mathbb{E}^{\gamma_0} \left(F(\Phi_{T_{j+1}^{(i)}}) \xi_{i,j+1} \mathbb{1}(\sigma_{j+1}^{(i)} \leq n_{i+1} - 3) \middle| \gamma_i \right).
\end{aligned}$$

However, if we condition on the σ -algebra $\mathcal{F}_{\sigma_{j+1}^{(i)}}^Y$, the σ -algebra generated by the Y components of the sequence $H_m^{(i)}$ up to the stopping time $\sigma_{j+1}^{(i)}$, then from Lemma A.2 we know that the distribution of $\Phi_{T_{j+1}^{(i)}}$ is a bridge segment starting according to π_γ and ending according to ν . This conditional expectation is therefore constant over j . Thus, we can write:

$$\begin{aligned}
\mathbb{E}^{\gamma_0} \left(\xi_{i,j} \xi_{i,j+1} \mathbb{1}(\sigma_{j+1}^{(i)} \leq n_{i+1} - 3) \middle| \gamma_i \right) &= \mathbb{E}^{\gamma_0} \left(F(\Phi_{T_{j+1}^{(i)}}) \xi_{i,j+1} \middle| \gamma_i \right) \\
&\quad \times \mathbb{P}^{\gamma_0}(\sigma_{j+1}^{(i)} \leq n_{i+1} - 3) \\
&= \mathbb{E}^{\gamma_0}(\xi_{i,j} \xi_{i,j+1} | \gamma_i) \mathbb{P}^{\gamma_0}(L_i - 1 \geq j + 1),
\end{aligned}$$

since $\xi_{i,j+1}$ is conditionally independent of $\{H_m^{(i)}\}_{m=0}^{\sigma_{j+1}^{(i)}}$.

Thus, we get that:

$$(B.18) \quad \sum_{j=1}^{\infty} \mathbb{E}^{\gamma_0} \left(\xi_{i,j} \xi_{i,j+1} \mathbb{1}(\sigma_{j+1}^{(i)} \leq n_{i+1} - 3) \middle| \gamma_i \right) = \mathbb{E}^{\gamma_0}(\xi_{i,1} \xi_{i,2} | \gamma_i) \mathbb{E}^{\gamma_0}(L_i - 2).$$

Combining Equations (B.16) and (B.18) gives:

$$(B.19) \quad \begin{aligned} \mathbb{E}^{\gamma_0}(\xi_i^2 | \gamma_i) &= \mathbb{E}^{\gamma_0}(\xi_{i,1}^2 | \gamma_i) \times \mathbb{E}^{\gamma_0}(L_i - 1) \\ &\quad + 2\mathbb{E}^{\gamma_0}(\xi_{i,1} \xi_{i,2} | \gamma_i) \times \mathbb{E}^{\gamma_0}(L_i - 2). \end{aligned}$$

For $\mathbb{E}^{\gamma_0}(L_i)$, we have that:

$$(B.20) \quad \mathbb{E}^{\gamma_0}(L_i) = 1 + \sum_{j=0}^{n_{i+1}-2} \mathbb{P}^{\gamma_0}(H_j^{(i)} \in \check{\alpha}) = 1 + \epsilon(n_{i+1} - 1),$$

for $i \geq 2$. The fixed value of $Y_0 = y$ will slightly skew the expectation of L_1 , but this is asymptotically irrelevant, or can be removed by taking $Y_0 \sim \text{Bern}(\epsilon)$.

We therefore get that:

$$(B.21) \quad \begin{aligned} \mathbb{E}^{\gamma_0}(\xi_i^2 | \gamma_i) &= \epsilon(n_{i+1} - 1) \mathbb{E}^{\gamma_0}(\xi_{i,1}^2 | \gamma_i) \\ &\quad + 2[\epsilon(n_{i+1} - 1) - 1] \mathbb{E}^{\gamma_0}(\xi_{i,1} \xi_{i,2} | \gamma_i) \\ &= (n_{i+1} - 1) \sigma^2(\gamma_i) - 2\mathbb{E}^{\gamma_i}(\xi_{1,1} \xi_{1,2}). \end{aligned}$$

This leaves $\mathbb{E}^{\gamma_0}(\xi_i^4 | \gamma_i)$, for which we rely on a crude upper bound using Doob's \mathcal{L}^p inequality. We have that:

$$(B.22) \quad \begin{aligned} \mathbb{E}^{\gamma_0}(\xi_i^4 | \gamma_i) &= \mathbb{E}^{\gamma_0} \left(\left[\sum_{j=1}^{L_i-1} \xi_{i,j} \right]^4 \middle| \gamma_i \right) \\ &\leq \mathbb{E}^{\gamma_0} \left(\max_{m=0, \dots, n_{i+1}-1} \left[\sum_{j=1}^m \xi_{i,j} \right]^4 \middle| \gamma_i \right). \end{aligned}$$

Since $\xi_{i,j}$ are conditionally 1-dependent, $\{\sum_{j=1}^m \xi_{i,j}\}_{m \geq 0}$ is not a martingale, even conditionally on γ_i . As in [4, Section 4], we can divide this sum into odd and even terms since:

$$(B.23) \quad \left[\sum_{j=1}^m \xi_{i,j} \right]^4 \leq 2^3 \left(\left[\sum_{\substack{j=1 \\ j \text{ odd}}}^m \xi_{i,j} \right]^4 + \left[\sum_{\substack{j=1 \\ j \text{ even}}}^m \xi_{i,j} \right]^4 \right),$$

by Jensen's inequality. These two sums are martingales because, conditionally on γ_i , $\{\xi_{i,2j}\}_{j \geq 1}$ and $\{\xi_{i,2j-1}\}_{j \geq 1}$ are iid sequences of mean 0 random variables. So we get that:

$$(B.24) \quad \begin{aligned} \mathbb{E}^{\gamma_0}(\xi_i^4 | \gamma_i) &\leq 8 \mathbb{E}^{\gamma_0} \left(\max_{m=0, \dots, n_{i+1}-1} \left[\sum_{\substack{j=1 \\ j \text{ odd}}}^m \xi_{i,j} \right]^4 \middle| \gamma_i \right) \\ &\quad + 8 \mathbb{E}^{\gamma_0} \left(\max_{m=0, \dots, n_{i+1}-1} \left[\sum_{\substack{j=1 \\ j \text{ even}}}^m \xi_{i,j} \right]^4 \middle| \gamma_i \right) \\ &\leq 8 \left(\frac{4}{3} \right)^4 \times \mathbb{E}^{\gamma_0} \left(\left[\sum_{\substack{j=1 \\ j \text{ odd}}}^{n_{i+1}-1} \xi_{i,j} \right]^4 + \left[\sum_{\substack{j=1 \\ j \text{ even}}}^{n_{i+1}-1} \xi_{i,j} \right]^4 \middle| \gamma_i \right), \end{aligned}$$

by Doob's \mathcal{L}^p inequality.

By conditional independence, we have that:

$$\begin{aligned} \mathbb{E}^{\gamma_0} \left(\left[\sum_{\substack{j=1 \\ j \text{ odd}}}^{n_{i+1}-1} \xi_{i,j} \right]^4 \middle| \gamma_i \right) &= \left\lceil \frac{n_{i+1}-1}{2} \right\rceil \mathbb{E}^{\gamma_i}(\xi_{1,1}^4) \\ &\quad + \left\lceil \frac{n_{i+1}-1}{2} \right\rceil \left(\left\lceil \frac{n_{i+1}-1}{2} \right\rceil - 1 \right) \mathbb{E}^{\gamma_i}(\xi_{1,1}^2)^2, \\ \mathbb{E}^{\gamma_0} \left(\left[\sum_{\substack{j=1 \\ j \text{ even}}}^{n_{i+1}-1} \xi_{i,j} \right]^4 \middle| \gamma_i \right) &= \left\lfloor \frac{n_{i+1}-1}{2} \right\rfloor \mathbb{E}^{\gamma_i}(\xi_{1,1}^4) \\ &\quad + \left\lfloor \frac{n_{i+1}-1}{2} \right\rfloor \left(\left\lfloor \frac{n_{i+1}-1}{2} \right\rfloor - 1 \right) \mathbb{E}^{\gamma_i}(\xi_{1,1}^2)^2. \end{aligned}$$

Substituting these into Equation (B.24) simplifies to give:

$$\begin{aligned} \mathbb{E}^{\gamma_0}(\xi_i^4 | \gamma_i) &\leq \frac{2048}{81} \left((n_{i+1}-1) \mathbb{E}^{\gamma_i}(\xi_{1,1}^4) + \frac{(n_{i+1}-2)^2}{2} \mathbb{E}^{\gamma_i}(\xi_{1,1}^2)^2 \right) \\ \text{(B.25)} \quad &= \mathcal{O}(n_{i+1}^2), \end{aligned}$$

uniformly over γ_i , assuming that $\sup_{\gamma \in \Gamma} \left(\mathbb{E}^{\gamma}(\xi_{1,1}^4) \right) < +\infty$, which follows from the fact that f is bounded and $\check{\sigma}_1 \sim \text{Geom}(\epsilon)$. \square

For the asymptotic results, the vast majority of our process is contained within the $\Xi_k^{(2)}$ terms, so we shall start by considering those.

LEMMA B.2 (\mathcal{L}^2 Convergence of $\Xi^{(2)}$). *Consider $\Xi_k^{(2)}$ as given in Equation (B.8). Then, assuming $\mathbb{E}_{\pi_\gamma}(f(X)) = 0$ for all $\gamma \in \Gamma$, we have that $\forall (\phi, y) \in \check{\Omega}$ and $\gamma_0 \in \Gamma$:*

$$\mathbb{E}^{\gamma_0}(\Xi_k^{(2)}) = 0,$$

and:

$$\mathbb{E}^{\gamma_0} \left(\left[\frac{1}{N_K} \Xi_k^{(2)} \right]^2 \right) = \mathcal{O} \left(\frac{1}{N_k} \right),$$

as $k \rightarrow +\infty$.

The proof of this Lemma follows relatively easily from Lemma B.1.

PROOF OF LEMMA B.2. The fact that $\mathbb{E}^{\gamma_0}(\Xi_k^{(2)}) = 0$ follows directly from the fact that $\mathbb{E}^{\gamma_0}(\xi_i) = 0$.

For $\mathbb{E}^{\gamma_0} \left(\left[\frac{1}{N_k} \Xi_k^{(2)} \right]^2 \right)$, we start by noting that:

$$\text{(B.26)} \quad \mathbb{E}^{\gamma_0}(\xi_i \xi_j) = 0,$$

for every $i \neq j$, which follows from a conditioning argument. Thus:

$$\text{(B.27)} \quad \mathbb{E}^{\gamma_0} \left((\Xi_k^{(2)})^2 \right) = \sum_{i=0}^{k-1} \mathbb{E}^{\gamma_0}(\xi_i^2).$$

Since $\sigma^2(\gamma)$ and $\mathbb{E}^\gamma(\xi_{1,1}^2)$ are bounded uniformly over $\gamma \in \Gamma$, we have that:

$$\begin{aligned} \mathbb{E}^{\gamma_0}(\xi_i^2) &\leq (n_{i+1} - 1)\mathbb{E}^{\gamma_0}(\sigma^2(\gamma_i)) + 2|\mathbb{E}^{\gamma_0}(\xi_{i,1}\xi_{i,2})| \\ (B.28) \quad &\leq (n_{i+1} - 1)\sup_{\gamma \in \Gamma}(\sigma^2(\gamma)) + 2\sup_{\gamma \in \Gamma}(\mathbb{E}^\gamma(\xi_{1,1}^2)). \end{aligned}$$

By Equation (B.27), this gives:

$$\begin{aligned} \mathbb{E}^{\gamma_0}\left(\left(\Xi_k^{(2)}\right)^2\right) &= \sum_{i=0}^{k-1} \mathbb{E}^{\gamma_0}(\xi_i^2) \leq (N_k - k)\sup_{\gamma \in \Gamma}(\sigma^2(\gamma)) \\ (B.29) \quad &\quad + 2k\sup_{\gamma \in \Gamma}(\mathbb{E}^\gamma(\xi_{1,1}^2)), \end{aligned}$$

so:

$$\begin{aligned} \mathbb{E}^{\gamma_0}\left(\left(\frac{1}{N_k}\Xi_k^{(2)}\right)^2\right) &\leq \sup_{\gamma \in \Gamma}(\sigma^2(\gamma))\left[\frac{k}{N_k^2} + \frac{1}{N_k}\right] \\ &\quad + \frac{2k}{N_k^2}\sup_{\gamma \in \Gamma}(\mathbb{E}^\gamma(\xi_{1,1}^2)) \\ (B.30) \quad &= \mathcal{O}\left(\frac{1}{N_k}\right), \end{aligned}$$

as required, since $N_k \geq k$. □

With this bound on second moments, we can move onto a CLT for $\Xi_k^{(2)}$.

LEMMA B.3 (Central Limit Theorem for $\Xi_k^{(2)}$). *Consider $\Xi_k^{(2)}$ as given in Equation (B.8). Assume $\mathbb{E}_\pi(f(X)) = 0$, and that $\sigma^2(\gamma)$ is a continuous function of γ . Suppose also that $\gamma_i \xrightarrow{P} \gamma_\infty$ as $i \rightarrow +\infty$, where γ_∞ is constant. Then, if $\sigma^2(\gamma_\infty) > 0$, we have that $\forall(\phi, y) \in \check{\Omega}, \gamma_0 \in \Gamma$:*

$$\frac{1}{\sqrt{N_k}}\Xi_k^{(2)} \xrightarrow{D} \mathcal{N}(0_d, \sigma^2(\gamma_\infty))$$

as $k \rightarrow +\infty$.

We will show later, using results following from Lemma B.2 and others, that the assumptions on the convergence of γ_i are not particularly restrictive for well chosen parameter estimators.

We follow a similar proof to the CLT proof for $\Xi_k^{(2)}$ in [12], based on Theorem 2.2 from [16].

PROOF OF LEMMA B.3. We apply Theorem 2.2 from [16] with $X_{n,k} = \frac{1}{\sqrt{N_n\sigma^2(\gamma_n)}}\xi_k$, though our indices do not quite line up with theirs.

Let:

$$(B.31) \quad \tilde{\mathcal{F}}_{-1} = \sigma(\gamma_0), \quad \tilde{\mathcal{F}}_i = \sigma\left(\tilde{\mathcal{F}}_{i-1} \cup \{\xi_{i,j}\}_{j \geq 1} \cup \{\gamma_{i+1}\}\right),$$

for $i \geq 0$. From Lemma B.1, we have $\mathbb{E}^{\gamma_0}(\xi_i | \tilde{\mathcal{F}}_{i-1}) = \mathbb{E}^{\gamma_0}(\xi_i | \gamma_i) = 0$, which gives condition (2.3) from [16].

Also by Lemma B.1, we have that:

$$(B.32) \quad \mathbb{E}^{\gamma_0}(\xi_i^2 | \tilde{\mathcal{F}}_{i-1}) = \mathbb{E}^{\gamma_0}(\xi_i^2 | \gamma_i) = (n_{i+1} - 1)\sigma^2(\gamma_i) - 2\mathbb{E}^{\gamma_i}(\xi_{1,1}\xi_{1,2}).$$

This gives that:

$$(B.33) \quad \sum_{i=0}^{k-1} \mathbb{E}^{\gamma_0}(\xi_i^2 | \tilde{\mathcal{F}}_{i-1}) = \sum_{i=0}^{k-1} (n_{i+1} - 1)\sigma^2(\gamma_i) - 2 \sum_{i=0}^{k-1} \mathbb{E}^{\gamma_i}(\xi_{1,1}\xi_{1,2}).$$

Assuming that $\gamma_i \xrightarrow{P} \gamma_\infty$ as $i \rightarrow +\infty$, and assuming that $\sigma^2(\gamma)$ is continuous in γ , we get that $\sigma^2(\gamma_i) \xrightarrow{P} \sigma^2(\gamma_\infty)$ as $i \rightarrow +\infty$. Since $\sigma^2(\gamma)$ is uniformly bounded, it follows also that $\sigma^2(\gamma_i) \xrightarrow{\mathcal{L}^1} \sigma^2(\gamma_\infty)$ as $i \rightarrow +\infty$.

From this, it is easy to show that:

$$(B.34) \quad \frac{1}{N_k} \sum_{i=0}^{k-1} \mathbb{E}^{\gamma_0}(\xi_i^2 | \tilde{\mathcal{F}}_{i-1}) \xrightarrow{\mathcal{L}^1} \sigma^2(\gamma_\infty), \quad \text{as } k \rightarrow +\infty,$$

which implies condition (2.4) from [16].

It remains for us to show the following Lindeberg condition:

$$(B.35) \quad \frac{1}{N_k} \sum_{i=0}^{k-1} \mathbb{E}^{\gamma_0}(\xi_i^2 \mathbb{1}(\xi_i^2 > \delta N_k) | \tilde{\mathcal{F}}_{i-1}) \xrightarrow{P} 0,$$

as $k \rightarrow +\infty$, for every $\delta > 0$.

Now, we can apply the Cauchy-Schwartz inequality and Markov's inequality to get that:

$$\begin{aligned} \mathbb{E}^{\gamma_0}(\xi_i^2 \mathbb{1}(\xi_i^2 > \delta N_k) | \tilde{\mathcal{F}}_{i-1}) &= \mathbb{E}^{\gamma_0}(\xi_i^2 \mathbb{1}(\xi_i^2 > \delta N_k) | \gamma_i) \\ &\leq \mathbb{E}^{\gamma_0}(\xi_i^4 | \gamma_i)^{1/2} \times \mathbb{P}^{\gamma_0}(\xi_i^2 > \delta N_k | \gamma_i)^{1/2} \\ &\leq \mathbb{E}^{\gamma_0}(\xi_i^4 | \gamma_i)^{1/2} \left[\frac{\mathbb{E}^{\gamma_0}(\xi_i^4 | \gamma_i)}{\delta^2 N_k^2} \right]^{1/2} \\ &= \frac{1}{\delta N_k} \mathbb{E}^{\gamma_0}(\xi_i^4 | \gamma_{i-1}). \end{aligned}$$

By Lemma B.1, we get that $\exists M > 0$ such that:

$$(B.36) \quad \frac{1}{N_k} \sum_{i=0}^{k-1} \mathbb{E}^{\gamma_0}(\xi_i^2 \mathbb{1}(\xi_i^2 > \delta N_k) | \tilde{\mathcal{F}}_{i-1}) \leq \frac{M \sum_{i=0}^{k-1} n_{i+1}^2}{\delta N_k^2},$$

which goes to 0 as $k \rightarrow +\infty$ by Lemma 1 from [12].

Thus, by Theorem 2.2 from [16], we get that:

$$(B.37) \quad \frac{1}{\sqrt{N_k \sigma^2(\gamma_k)}} \Xi_k^{(2)} \xrightarrow{D} \mathcal{N}(0, 1),$$

which gives the required result since $\sigma^2(\gamma_k) \xrightarrow{P} \sigma^2(\gamma_\infty)$. \square

B.2. Controlling the Other Terms. We now turn to the remaining terms in Equation (B.8).

LEMMA B.4 (Moments of $\Xi_k^{(1)}$, $\Xi_k^{(3)}$ and $\Xi_{k,N}^{(4)}$). *Consider $\Xi_k^{(1)}$, $\Xi_k^{(3)}$ and $\Xi_{k,N}^{(4)}$ as given in Equation (B.8). Then, assuming $\mathbb{E}_\pi(f(X)) = 0$ for f bounded, we have that $\forall(\phi, y) \in \check{\Omega}$ and $\gamma_0 \in \Gamma$:*

$$\mathbb{E}_{(\phi,y)}^{\gamma_0}([\Xi_k^{(1)}]^2) = \mathcal{O}(k^2), \quad \mathbb{E}_{(\phi,y)}^{\gamma_0}([\Xi_k^{(3)}]^2) = \mathcal{O}(k^2),$$

and:

$$\mathbb{E}_{(\phi,y)}^{\gamma_0}([\Xi_{k,N}^{(4)}]^2) = \mathcal{O}(n_{k+1}).$$

The proof of this Lemma follows from Jensen's inequality for $\Xi_k^{(1)}$ and $\Xi_k^{(3)}$, and from a regeneration argument for $\Xi_{k,N}^{(4)}$.

PROOF OF LEMMA B.4. By Jensen's inequality, we have that:

$$\begin{aligned} \mathbb{E}_{(\phi,y)}^{\gamma_0}([\Xi_k^{(1)}]^2) &= \mathbb{E}_{(\phi,y)}^{\gamma_0} \left(\left[\sum_{i=0}^{k-1} \eta_i \right]^2 \right) \\ &\leq k \sum_{i=0}^{k-1} \mathbb{E}_{(\phi,y)}^{\gamma_0}(\eta_i^2) \\ &= k \sum_{i=0}^{k-1} \mathbb{E}_{(\phi,y)}^{\gamma_0} \left(\left[\sum_{j=0}^{T_1^{(i)}} F(H_j^{(i)}) \right]^2 \right) \\ (B.38) \quad &\leq k^2 M^2 \mathbb{E}((\check{T}_1 + 1)^2), \end{aligned}$$

where $|f| \leq M$, and since $T_1^{(i)} \sim \text{Geom}(\epsilon)$ for each i .

Since the renewal sequence $\{T_j^{(i)}\}_{j \geq 1}$ has $\text{Geom}(\epsilon)$ increments and is therefore memoryless, an identical argument gives that:

$$(B.39) \quad \mathbb{E}_{(\phi,y)}^{\gamma_0}([\Xi_k^{(3)}]^2) \leq k^2 M^2 \mathbb{E}((\check{T}_1 + 1)^2).$$

Now, for $\mathbb{E}_{(\phi,y)}^{\gamma_0}([\Xi_{k,N}^{(4)}]^2)$, we follow an identical argument to Lemma B.1. Setting:

$$(B.40) \quad L^{(4)} = L^{(4)}(k, N) = \inf(l \geq 1 : T_l^{(k+1)} \geq N - N_k - 1),$$

we write:

$$\begin{aligned} (B.41) \quad \eta^{(4)} &= \sum_{j=0}^{T_1^{(k+1)}} F(H_j^{(k+1)}), & \xi^{(4)} &= \sum_{j=T_1^{(k+1)}+1}^{T_{L^{(4)}}^{(k+1)}} F(H_j^{(k+1)}) \\ \zeta^{(4)} &= \sum_{j=N-N_k}^{T_{L^{(4)}}^{(k+1)}} F(H_j^{(k+1)}), & \xi_{i,j}^{(4)} &= \sum_{m=T_j^{(k+1)}+1}^{T_{j+1}^{(k+1)}} F(H_m^{(k+1)}). \end{aligned}$$

We can therefore divide $\Xi_{k,N}^{(4)}$ as:

$$(B.42) \quad \Xi_{k,N}^{(4)} = \eta^{(4)} + \xi^{(4)} - \zeta^{(4)},$$

as we did for s_i in Equation (B.7). Now, by an identical argument to Equations (B.38) and (B.39), we get that:

$$(B.43) \quad \mathbb{E}_{(\phi,y)}^{\gamma_0}([\eta^{(4)}]^2) = \mathcal{O}(1), \quad \mathbb{E}_{(\phi,y)}^{\gamma_0}([\zeta^{(4)}]^2) = \mathcal{O}(1),$$

and by an identical argument to Lemma B.1, we get that:

$$(B.44) \quad \mathbb{E}_{(\phi,y)}^{\gamma_0}([\xi^{(4)}]^2) = \mathcal{O}(N - N_k) \implies \mathbb{E}_{(\phi,y)}^{\gamma_0}([\xi^{(4)}]^2) = \mathcal{O}(n_{k+1}).$$

Using these bounds and Equation (B.42) therefore gives:

$$(B.45) \quad \mathbb{E}_{(\phi,y)}^{\gamma_0}([\Xi_{k,N}^{(4)}]^2) = \mathcal{O}(n_{k+1}),$$

which completes the proof. \square

B.3. Gathering all the Terms. We can now conclude by gathering all the terms. This will yield the results given in Theorem 4.5.

Recall first of all that, from Equation (3.5), we are assuming that $n_k = \Theta(k^\beta)$, which implies $N_k = \Theta(k^{\beta+1})$. We can start by gathering our bounds from Lemma B.1 and B.4 to show the following:

THEOREM B.5 (Segment Chain \mathcal{L}^2 convergence). *Consider $(\Phi_n, Y_n)_{n \geq 0}$ the AIR segment chain process, where the original family of transition kernels $\{P_\gamma\}_{\gamma \in \Gamma}$ have invariant distributions π_γ and satisfy the minorisation condition (4.1). Assume that f is bounded and $\mathbb{E}_{\pi_\gamma}(f(X)) = 0$ for all $\gamma \in \Gamma$. Then $\forall (\Phi_0, Y_0) \in \check{\Omega}$, $\gamma_0 \in \Gamma$, and any adaptation scheme: For any $\beta > 0$,*

$$\mathbb{E}_{(\Phi_0, Y_0)}^{\gamma_0} \left(\left[\frac{1}{N} S_N \right]^2 \right) = \mathcal{O} \left(N^{-\min(1, \frac{2\beta}{1+\beta})} \right),$$

so that \mathcal{L}^2 convergence holds.

The proof of this theorem is simply a matter of gathering terms from previous results, and is identical to the proof of Theorem 1 from [12]. Rearranging the terms yields the expression in Theorem 4.5.

PROOF OF THEOREM B.5. For the \mathcal{L}^2 convergence, note that by Lemma B.1 and B.4, we have:

$$\mathbb{E}_{(\Phi_0, Y_0)}^{\gamma_0} \left(\left[\frac{1}{N_k} S_N \right]^2 \right) = \mathcal{O} \left(\frac{1}{N_k} \right) + \mathcal{O} \left(\frac{k^2}{N_k^2} \right) + \mathcal{O} \left(\frac{n_{k+1}}{N_k^2} \right).$$

Since $\frac{N_k}{N} \rightarrow 1$ as $N \rightarrow +\infty$, and n_k, N_k are of order k^β and $k^{\beta+1}$ respectively, we get that:

$$\mathbb{E}_{(\Phi_0, Y_0)}^{\gamma_0} \left(\left[\frac{1}{N} S_N \right]^2 \right) = \mathcal{O}(N^{-1}) + \mathcal{O} \left(N^{-\frac{2\beta}{\beta+1}} \right),$$

which gives the \mathcal{L}^2 convergence. \square

Finally, we prove the central limit theorem for S_N .

THEOREM B.6 (Central Limit Theorem for AIR SBPS). *Suppose $\beta > 1$. Consider $(\Phi_n, Y_n)_{n \geq 0}$ the AIR segment chain process, where the original family of transition kernels $\{P_\gamma\}_{\gamma \in \Gamma}$ have invariant distributions π_γ and satisfy the minorisation condition (4.1). Assume*

that f is bounded and $\mathbb{E}_{\pi_\gamma}(f(X)) = 0$ for all $\gamma \in \Gamma$. Then, if $\gamma_i \xrightarrow{P} \gamma_\infty$ such that $\sigma^2(\gamma_\infty) > 0$, and that $\sigma^2(\gamma)$ is a continuous function of γ , then $\forall(\Phi_0, Y_0) \in \tilde{\Omega}$, $\gamma_0 \in \Gamma$:

$$\frac{1}{\sqrt{N}} S_N \xrightarrow{D} \mathcal{N}(0, \sigma^2(\gamma_\infty)).$$

This theorem follows immediately from Lemma B.3's CLT for $\frac{1}{\sqrt{N_k}} \Xi_k^{(2)}$, then using the moment bounds in Lemma B.4 to show that the other terms go to 0 in probability for large N , assuming $\beta > 1$.

Funding. Cameron Bell has been supported by the EPSRC on studentship grant EP/W523793/1.

Krzysztof Łatuszyński has been supported by the Royal Society through the Royal Society University Research Fellowship.

Gareth O. Roberts has been supported by the UKRI grant EP/Y014650/1 as part of the ERC Synergy project OCEAN, EPSRC grants Bayes for Health (R018561), CoSiNES (R034710), PINCODE (EP/X028119/1), and EP/V009478/1.

SUPPLEMENTARY MATERIAL

All code used for simulations can be found in our github repository:
<https://github.com/tamarock143/Julia-Stereographic>.

REFERENCES

- [1] ANDRAL, C. and KAMATANI, K. (2024). Automated Techniques for Efficient Sampling of Piecewise-Deterministic Markov Processes. *arXiv preprint arXiv:2408.03682*.
- [2] ANDRIEU, C. and MOULINES, E. (2006). On the ergodicity properties of some adaptive MCMC algorithms. *Ann. Appl. Probab.* **16** 1462–1505. <https://doi.org/10.1214/105051606000000286> MR2260070
- [3] ANDRIEU, C. and THOMS, J. (2008). A tutorial on adaptive MCMC. *Stat. Comput.* **18** 343–373. <https://doi.org/10.1007/s11222-008-9110-y> MR2461882
- [4] BEDNORZ, W., ŁATUSZYŃSKI, K. and LATAŁ, A. R. (2008). A regeneration proof of the central limit theorem for uniformly ergodic Markov chains. *Electron. Commun. Probab.* **13** 85–98. <https://doi.org/10.1214/ECP.v13-1354> MR2386065
- [5] BERTAZZI, A. and BIERKENS, J. (2022). Adaptive schemes for piecewise deterministic Monte Carlo algorithms. *Bernoulli* **28** 2404–2430. <https://doi.org/10.3150/21-bej1423> MR4474548
- [6] BIERKENS, J. and DUNCAN, A. (2017). Limit theorems for the zig-zag process. *Advances in Applied Probability* **49** 791–825.
- [7] BIERKENS, J., FEARNHEAD, P. and ROBERTS, G. (2019). The zig-zag process and super-efficient sampling for Bayesian analysis of big data. *Ann. Statist.* **47** 1288–1320. <https://doi.org/10.1214/18-AOS1715> MR3911113
- [8] BIERKENS, J., KAMATANI, K. and ROBERTS, G. O. (2022). High-dimensional scaling limits of piecewise deterministic sampling algorithms. *The Annals of Applied Probability* **32** 3361–3407.
- [9] BIERKENS, J., GRAZZI, S., KAMATANI, K. and ROBERTS, G. (2020). The boomerang sampler. In *International conference on machine learning* 908–918. PMLR.
- [10] BOUCHARD-CÔTÉ, A., VOLLMER, S. J. and DOUCET, A. (2018). The bouncy particle sampler: A nonreversible rejection-free Markov chain Monte Carlo method. *Journal of the American Statistical Association* **113** 855–867.
- [11] CHIMISOV, C., ŁATUSZYŃSKI, K. and ROBERTS, G. (2018). Adapting the Gibbs sampler. *arXiv preprint arXiv:1801.09299*.
- [12] CHIMISOV, C., ŁATUSZYŃSKI, K. and ROBERTS, G. O. (2018). Air Markov chain Monte Carlo. *arXiv preprint arXiv:1801.09309*.
- [13] CORBELLA, A., SPENCER, S. E. F. and ROBERTS, G. O. (2022). Automatic Zig-Zag sampling in practice. *Stat. Comput.* **32** Paper No. 107, 16. <https://doi.org/10.1007/s11222-022-10142-x> MR4507158

- [14] DELIGIANNIDIS, G., BOUCHARD-CÔTÉ, A. and DOUCET, A. (2019). Exponential ergodicity of the bouncy particle sampler. *Ann. Statist.* **47** 1268–1287. <https://doi.org/10.1214/18-AOS1714> MR3911112
- [15] DOWN, D., MEYN, S. P. and TWEEDIE, R. L. (1995). Exponential and uniform ergodicity of Markov processes. *Ann. Probab.* **23** 1671–1691. MR1379163
- [16] DVORETZKY, A. (1972). Asymptotic normality for sums of dependent random variables. In *Proceedings of the Sixth Berkeley Symposium on Mathematical Statistics and Probability, Volume 2: Probability Theory* **6** 513–536. University of California Press.
- [17] FORT, G., MOULINES, E. and PRIOURET, P. (2011). Convergence of adaptive and interacting Markov chain Monte Carlo algorithms. *Ann. Statist.* **39** 3262–3289. <https://doi.org/10.1214/11-AOS938> MR3012408
- [18] GILKS, W. R., ROBERTS, G. O. and SAHU, S. K. (1998). Adaptive Markov chain Monte Carlo through regeneration. *J. Amer. Statist. Assoc.* **93** 1045–1054. <https://doi.org/10.2307/2669848> MR1649199
- [19] GIROLAMI, M. and CALDERHEAD, B. (2011). Riemann manifold langevin and hamiltonian monte carlo methods. *Journal of the Royal Statistical Society Series B: Statistical Methodology* **73** 123–214.
- [20] HABECK, M., HASENPFLUG, M., KODGIRWAR, S. and RUDOLF, D. (2023). Geodesic slice sampling on the sphere. *arXiv preprint arXiv:2301.08056*.
- [21] HASTINGS, W. K. (1970). Monte Carlo sampling methods using Markov chains and their applications. *Biometrika* **57** 97–109. <https://doi.org/10.1093/biomet/57.1.97> MR3363437
- [22] HOFFMAN, M. D. and GELMAN, A. (2014). The no-U-turn sampler: adaptively setting path lengths in Hamiltonian Monte Carlo. *J. Mach. Learn. Res.* **15** 1593–1623. MR3214779
- [23] HOFSTADLER, J., LATUSZYŃSKI, K., ROBERTS, G. O. and RUDOLF, D. (2024). Almost sure convergence rates of adaptive increasingly rare Markov chain Monte Carlo. *arXiv preprint arXiv:2402.12122*.
- [24] JOHNSON, L. T. and GEYER, C. J. (2012). Variable transformation to obtain geometric ergodicity in the random-walk Metropolis algorithm. *The Annals of Statistics* 3050–3076.
- [25] METROPOLIS, N., ROSENBLUTH, A. W., ROSENBLUTH, M. N., TELLER, A. H. and TELLER, E. (1953). Equation of state calculations by fast computing machines. *The journal of chemical physics* **21** 1087–1092.
- [26] MEYN, S. P. and TWEEDIE, R. L. (2012). *Markov chains and stochastic stability*. Springer Science & Business Media.
- [27] NEAL, R. M. (2011). MCMC Using Hamiltonian Dynamics. In *Handbook of Markov Chain Monte Carlo* 139–188. Chapman and Hall/CRC.
- [28] POMPE, E., HOLMES, C. and ŁATUSZYŃSKI, K. (2020). A framework for adaptive MCMC targeting multimodal distributions. *Ann. Statist.* **48** 2930–2952. <https://doi.org/10.1214/19-AOS1916> MR4152629
- [29] REVELS, J., LUBIN, M. and PAPAMARKOU, T. (2016). Forward-mode automatic differentiation in Julia. *arXiv preprint arXiv:1607.07892*.
- [30] ROBERTS, G. O., GELMAN, A. and GILKS, W. R. (1997). Weak convergence and optimal scaling of random walk Metropolis algorithms. *Ann. Appl. Probab.* **7** 110–120. <https://doi.org/10.1214/aoap/1034625254> MR1428751
- [31] ROBERTS, G. O. and ROSENTHAL, J. S. (2007). Coupling and ergodicity of adaptive Markov chain Monte Carlo algorithms. *J. Appl. Probab.* **44** 458–475. <https://doi.org/10.1239/jap/1183667414> MR2340211
- [32] ROBERTS, G. O. and ROSENTHAL, J. S. (2009). Examples of adaptive MCMC. *J. Comput. Graph. Statist.* **18** 349–367. <https://doi.org/10.1198/jcgs.2009.06134> MR2749836
- [33] SAKSMAN, E. and VIHOLA, M. (2010). On the ergodicity of the adaptive Metropolis algorithm on unbounded domains. *Ann. Appl. Probab.* **20** 2178–2203. <https://doi.org/10.1214/10-AAP682> MR2759732
- [34] SYED, S., BOUCHARD-CÔTÉ, A., DELIGIANNIDIS, G. and DOUCET, A. (2022). Non-reversible parallel tempering: a scalable highly parallel MCMC scheme. *J. R. Stat. Soc. Ser. B. Stat. Methodol.* **84** 321–350. MR4412989
- [35] TAWN, N. G., MOORES, M. T. and ROBERTS, G. O. (2021). Annealed Leap-Point Sampler for multimodal target distributions. *arXiv preprint arXiv:2112.12908*.
- [36] VASDEKIS, G. and ROBERTS, G. O. (2023). Speed up zig-zag. *The Annals of Applied Probability* **33** 4693–4746.
- [37] YANG, J., ŁATUSZYŃSKI, K. and ROBERTS, G. O. (2024). Stereographic Markov Chain Monte Carlo. *The Annals of Statistics* **52** 2692–2713.